Interaction of wave with a body floating on a wide polynya

Z.F. Li [a], Y.Y. Shi [b], and G.X. Wu [a,c,*]

[a] School of Naval Architecture and Ocean Engineering, Jiangsu University of Science and Technology, Zhenjiang 212003, China

[b] College of Shipbuilding Engineering, Harbin Engineering University, Harbin 150001, China

[c] Department of Mechanical Engineering, University College London, Torrington Place, London WC1E 7JE, UK

Abstract

A method based on wide spacing approximation is proposed for the interaction of water wave with a body floating on a polynya. The ice sheet is modelled as an elastic plate and fluid flow is described by the velocity potential theory. The solution procedure is constructed based on the assumption that when the distance between two disturbances to the free surface is sufficiently large, the interactions between them involve only the travelling waves caused by the disturbances and the effect of the evanescent waves is ignored. The solution for the problem can then be obtained from those for a floating body without ice sheet and for ice sheet/free surface without floating body. Both latter solutions have already been found previously and therefore there will be no additional effort in solution once the wide spacing approximation formulation is derived. Extensive numerical results are provided to show that the method is very accurate compared with the exact solution. The obtained formulations are then used to provide some insightful explanations for the physics of flow behaviour, as well as the mechanism for the highly oscillatory features of the hydrodynamic force and body motion. Some explicit equations are derived to show zero reflection by the polynya, and peaks and troughs of the force and excited body motion. It is revealed that some of the peaks of the body motion are due to resonance while others are to the wave characters in the polynya.

Key words: ice sheet; wide polynya; floating body; highly oscillatory hydrodynamic force; body motion resonance and multi peaks response

I. INTRODUCTION

Interaction of water wave with a floating body has been of great interest due to the complexity of

[*] Corresponding author. Permanent address: Department of Mechanical Engineering, University College London, Torrington Place, London WCIE 7JE, UK. Tel.: +44 20 7679 3870; fax: +44 20 7388 0180.
E-mail address: g.wu@ucl.ac.uk (G.X. Wu)

flow features and its practical relevance, in particular to ocean and coastal engineering, as well as naval architecture. The ocean surface is usually treated as infinitely large, on which the pressure is assumed to be atmospheric, and it is commonly refereed as the free surface when the atmospheric pressure is taken as constant. The research over the last decades has significantly advanced our understanding of the nature of the wave physics and the mechanism of its interaction with a floating body. The latest development in Arctic engineering, in particular the possibility of new shipping routes in the next few decades, has led to some new technical challenges. One of such challenges arises when a ship navigates through a strip of water confined between large ice sheets, which could be formed through melting of Arctic ice [1] or opened up by an icebreaker [2]. The flow and body motion features will be different from those in open sea and will very much depend on the wave/ice/body interaction. A better understanding of these features is highly important for safety, environmental protection as well as economic cost.

The observations by Robin[3] suggested a large ice sheet could be treated as an elastic plate in the wave/ice interaction problems. This model has been widely used subsequently. A review of earlier work for this kind of problem was given by Squire *et al.*[4], and the more recent ones were given by Squire[5, 1]. A semi-infinite ice sheet on the free surface was considered based on the thin plate model by Fox and Squire[6] and based on the thick plate mode by Fox and Squire[7] using the matched eigenfunction expansion method. Numerical comparison showed that in terms of the reflection and transmission coefficients these two methods gave graphically indistinguishable results. The case was then extended to the oblique incident wave by Fox and Squire[8]. For the similar problems, Sahoo *et al.*[9] introduced an inner product of orthogonality and considered the ice sheets with various edge conditions. Meylan and Squire[10] adopted the Green function method which was more flexible and could be applied to a much wider range of problems. It is also possible to apply the Wiener-Hopf method for this type of problem[11]. Chung and Fox[12] used the method for the oblique reflection and transmission of ocean waves into the semi-infinite ice sheet. Other notable work using the Wiener-Hopf method include those by Balmforth and Craster[13] and by Tkacheva[14, 15]. Chung and Linton[16] considered wave reflection and transmission when propagating across a gap between two semi-infinite ice sheets, or polynya, and found that the reflection coefficient could be zero at discrete frequencies. Williams and Squire[17] solved the problem of interaction of wave with three connected plates of different thickness. When the thickness is taken zero, it becomes a free surface and thus the polynya can be treated as one of the special cases of such a problem. The problem of an imperfect ice sheet, with a crack for example, was investigated by Evans and Porter[18], Porter and Evans[19], and more recently by Sturova and

Tkacheva[20].

The above work is mainly about the interactions between ocean waves and ice sheets. For wave/ice/body interaction problems, Das and Mandal[21] studied the oblique wave scattering by a circular cylinder submerged beneath an ice cover through the multipole expansion method. Sturova[22] considered the problem of a submerged cylinder and the corresponding Green function satisfying all the boundary conditions apart from that on the body surface was derived. The method was then extended to the problem of two semi-infinite ice sheets connected by vertical and flexural rotational springs [23], and the ice floe or polynya [24]. For a floating body on the polynya, Ren *et al.*[25] obtained the semi-analytical solution based on the matched eigenfunction expansions for a rectangular box. Li *et al.*[26] considered the nonlinear effects of the body motion through a semi analytical solution for a circular cylinder in large amplitude oscillation. For general cases of body with arbitrary shapes, Li *et al.*[27] developed a hybrid method by combining the boundary element method and eigenfunction expansion method.

The problem described above have been mainly solved exactly in the sense when a discretization of the boundary is refined or the number of terms in an infinite series further increases, the numerical result no longer changes within the desired accuracy. We may also notice that the solution procedure for such a problem is much more complex than that for free surface without ice sheet or for ice sheet without free surface. This is reflected by the far more complex Green function for the wave/body/ice interaction problem [24]. Thus this has motivated the present work to develop an efficient yet highly accurate method.

Here we notice the fact that the wave generated/disturbed by the body or ice edge has two components. One is the evanescent wave which will decay exponentially away from the disturbance, while the other is the travelling wave which will propagate away from the disturbance to infinity. Thus when the locations of two disturbances are sufficiently large, only the latter needs to be considered in their interactions. Therefore, in this work by following the wide spacing approximation used in the multi bodies/wave interaction [28], we consider the problem of wave interaction with a body floating on a wide polynya. The wide approximation enables us to construct a solution based on those for the problem of a floating body without ice sheet and the problem of ice sheet/free surface without floating body. The merit of this method is that it can give an accurate solution based on what has already been solved previously. In the following sections, we shall first derive the formulation based on this method. Extensive numerical results are then provided, including the wave propagation across the polynya, and interaction with a submerged body and a floating body in polynya. The method is verified through the excellent agreement with the exact solution. The formulation is subsequently used to provide deep insights into the complex wave features, as well as hydrodynamic forces and body response to the waves.

II. MATHEMATICAL MODEL AND NUMERICAL PROCEDURES

A. Mathematical model

We consider the interaction problem of wave with a two dimensional body floating on a wide polynya confined between two semi-infinite ice sheets, as sketched in Fig. 1. A Cartesian coordinate system $\vec{x} = (x, z)$ fixed in space is chosen with the origin O at the undisturbed mean free surface, x being the horizontal direction, and z vertically upward. When the body is at its equilibrium position, the z-axis passes through the centre of its mass. In each side of the polynya, i.e. $x < x_1$ and $x > x_2$, the upper surface of the fluid is covered by a semi-infinite ice sheet. The width of the polynya is $l = x_2 - x_1$. The body with beam a and draught b respectively is assumed to be excited into motion by an incident wave propagating underneath the left ice sheet. The present work is undertaken on the basis that the gap between the edge of the ice to the body is much larger than the typical dimension of the body, or $l >> a$.

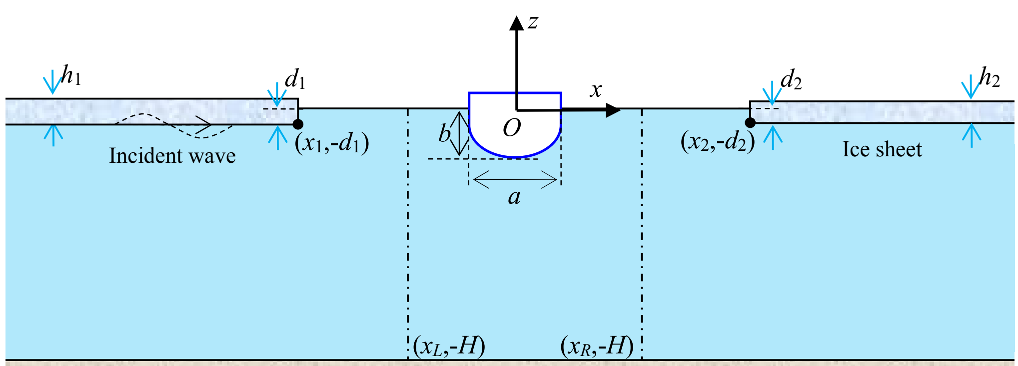

Fig. 1. Coordinate system and sketch of the problem.

The fluid with density ρ and constant depth H is assumed to be inviscid, incompressible and homogeneous, and its motion to be irrotational. Thus the velocity potential Φ can be introduced to describe the fluid flow. Under the assumption that the amplitude of wave motion is small compared to its length and the dimension of the body, the linearized velocity potential theory can be further used. When the motion is sinusoidal in time with radian frequency ω, the total potential can be written as [29]

$$\Phi(x,z,t) = \mathrm{Re}[\alpha_0 \phi_0(x,z)\mathrm{e}^{\mathrm{i}\omega t}] + \mathrm{Re}[\sum_{k=1}^{3} \mathrm{i}\omega \alpha_k \phi_k(x,z)\mathrm{e}^{\mathrm{i}\omega t}] \quad (1)$$

where ϕ_0 contains the incident potential ϕ_I and diffracted potential ϕ_D, α_0 is the amplitude of the incident wave; ϕ_k ($k = 1, 2, 3$) are the radiation potentials due to body oscillation with complex amplitude α_k in three degrees of freedom: translations in x and z directions respectively and rotation about y-axis parallel to the ice sheet edge. Mass conservation requires that the potential ϕ_k satisfies the Laplace's equation

$$\nabla^2\phi_k = 0, \; (k = 0, 1, 2, 3) \tag{2}$$

throughout the fluid. The combination of the linearized dynamic and kinematic free surface boundary conditions gives

$$-\omega^2\phi_k + g\frac{\partial\phi_k}{\partial z} = 0, \; (x_1 < x < x_2, \;\; z = 0) \tag{3}$$

where g is the acceleration due to gravity. The ice sheet is modelled as a continuous elastic plate with uniform properties, i.e. thickness h_j, draught d_j, density ρ_j, Young's modulus E_j, Poisson's ration ν_j are all constant. Thus the boundary condition on the ice sheets can be written as [6]

$$(L_j\frac{\partial^4}{\partial x^4} - m_j\omega^2 + \rho g)\frac{\partial\phi_k}{\partial z} - \rho\omega^2\phi_k = 0, \; (|x| \geq |x_j|, \;\; z = -d_j, \;\; j = 1, 2) \tag{4}$$

where $L_j = Eh_j^3/[12(1-\nu_j^{\,2})]$ is the effective flexural rigidity of the ice sheet, and $m_j = h_j\rho_j$ is its mass per unit area. Without loss of generality, the end of the ice sheet is assumed to be free here. Thus the vanishing of the bending moment and shear force leads to the following two conditions on the ice sheet edge corner

$$\frac{\partial^2}{\partial x^2}(\frac{\partial\phi_k}{\partial z}) = 0 \;\text{ and }\; \frac{\partial^3}{\partial x^3}(\frac{\partial\phi_k}{\partial z}) = 0, \; (x = x_j, \;\; z = -d_j) \tag{5}$$

On the vertical surface of the ice sheet, the impermeable condition yields

$$\frac{\partial\phi_k}{\partial x} = 0, \; (x = x_j, \;\; -d_j \leq z \leq 0) \tag{6}$$

The impermeable condition on the body surface is

$$\frac{\partial\phi_0}{\partial n} = 0 \;\text{ and }\; \frac{\partial\phi_k}{\partial n} = n_k, \; (k = 1, 2, 3) \tag{7}$$

where n_1 and n_2 are the x, z components of the unit normal vector $\vec{n}$ pointing into the body, $n_3 = (z-z')n_1 - (x-x')n_2$ is the component related to the rotational mode, with (x', z') as the rotational centre. The boundary condition on the flat seabed can be written as

$$\frac{\partial\phi_k}{\partial z} = 0, \; (-\infty < x < +\infty, \;\; z = -H) \tag{8}$$

The radiation condition requires the wave to propagate outwards

$$\lim_{x\to+\infty}(\frac{\partial\phi_k}{\partial x} + \kappa_0^{(2)}\phi_k) = 0, \;\; \lim_{x\to-\infty}(\frac{\partial\phi_k}{\partial x} - \kappa_0^{(1)}\phi_k) = 0, \; (k = 1, 2, 3) \tag{9}$$

$$\lim_{x\to+\infty}(\frac{\partial\phi_D}{\partial x} + \kappa_0^{(2)}\phi_D) = 0, \;\; \lim_{x\to-\infty}(\frac{\partial\phi_D}{\partial x} - \kappa_0^{(1)}\phi_D) = 0 \tag{10}$$

where $\kappa_0^{(1)}$ and $\kappa_0^{(2)}$ are the purely positive imaginary roots of the dispersion equations for the ice covered regions, or

$$-\kappa_0^{(j)}\tan[\kappa_0^{(j)}(H-d_j)]=\frac{\rho\omega^2}{L_j(\kappa_0^{(j)})^4+\rho g-m_j\omega^2},\ (j=1,2) \tag{11}$$

B. Hydrodynamic force and body motion

When the velocity potential ϕ_k is solved, the pressure can be obtained through the linearized Bernoulli equation, and the hydrodynamic force exerting on the body can be obtained directly by integrating the dynamic pressure over the mean wetted body surface. Based on the decomposition of the velocity potentials Eq. (1), the hydrodynamic force can be equivalently expressed as the wave exciting force due to unit wave amplitude

$$f_{E,k}=-\mathrm{i}\omega\rho\int_{S_0}\phi_0(x,z)n_k\mathrm{d}S \tag{12}$$

and the hydrodynamic coefficients

$$\mu_{kj}-\mathrm{i}\frac{\lambda_{kj}}{\omega}=\rho\int_{S_0}\phi_j n_k\mathrm{d}S \tag{13}$$

where μ_{kj} and λ_{kj} are the added mass and damping coefficient respectively.

Based on the Newton's law, and taking into account the hydrostatic force due to the variation of the buoyance during body oscillation, the complex motion amplitudes α_j ($j=1,\ 2,\ 3$) can be computed through the following linear equations

$$\sum_{j=1}^{3}[-\omega^2(m_{kj}+\mu_{kj})+\mathrm{i}\omega\lambda_{kj}+C_{kj}]\alpha_j=\alpha_0 f_{E,k},\quad k=1,\ 2,\ 3 \tag{14}$$

where $j=1,\ 2,\ 3$ represent the modes sway, heave and roll; m_{kj} and C_{kj} are respectively the body mass and hydrostatic restoring coefficients.

C. Solution procedure

The problem described in Eqs. (1) to (11) can be solved accurately through numerical methods generally. Here we shall use wide spacing approximation. To construct the expression for the solution, we denote the radiation and scattering velocity potentials of the body in the absence of ice sheets as ψ_k^r and $\psi_0^{s\pm}$ respectively, where $+$ and $-$ correspond to that the incident wave opposite to and along the *x*-axis respectively. We further consider the problem due to semi-infinite ice sheet and semi-infinite free surface, and define the velocity potentials as $\psi_{Ice,L}^{w2i}$ and $\psi_{Ice,R}^{w2i}$, where the superscript $w2i$ means that the incident wave is propagating from the open water to the ice covered region, and the subscripts L and R mean that the semi-infinite ice sheet is covered on the left and right hand sides of the upper surface respectively, i.e. $x\in(-\infty,0]$ and $x\in[0,+\infty)$. Corresponding to these two potentials, we also define $\psi_{Ice,L}^{i2w}$ and $\psi_{Ice,R}^{i2w}$, where $i2w$ means that the incident wave is propagating from the ice covered region to the open water.

The velocity potentials ψ_k^r and $\psi_0^{s\pm}$ satisfy the following boundary condition on the body surface

$$\frac{\partial \psi_k^r}{\partial n} = n_k \quad \text{and} \quad \frac{\partial \psi_0^{s\pm}}{\partial n} = 0\,,\ (k = 1, 2, 3) \tag{15}$$

and the boundary conditions in Eq. (3) and Eq. (8) respectively on the free surface and flat seabed. At infinity we have

$$\lim_{x\to\pm\infty}(\frac{\partial \psi_k^r}{\partial x} \pm k_0\psi_k^r) = 0\,,\ (k = 1, 2, 3) \tag{16}$$

$$\lim_{x\to\pm\infty}[\frac{\partial(\psi_0^{s\pm} - \psi_I)}{\partial x} \pm k_0(\psi_0^{s\pm} - \psi_I)] = 0 \tag{17}$$

where k_0 is the purely positive imaginary root of the dispersion equation for open water, or

$$-k_0 \tan(k_0 H) = \frac{\omega^2}{g} \tag{18}$$

and ψ_I is the incident potential in open water.

For the interaction problem of wave with the semi-infinite ice sheet, the velocity potential should satisfy the boundary conditions in Eqs. (3) and (4) respectively on the free surface and the ice sheet, and the boundary condition in Eq. (8) on the flat seabed. Also, the free edge condition in Eq. (5) should be satisfied. At infinity, the radiation conditions are the same as those in Eqs. (17) and (10), in the open water and ice covered region respectively.

Here we notice that the velocity potentials ψ_k^r and $\psi_0^{s\pm}$ are classic problems and have been solved previously, for example by the hybrid integral equation and eigenfunction expansion method [30], or the hybrid finite element and integral equation method [31]. Similarly the velocity potential $\psi_{Ice,L}^{w2i}$ and $\psi_{Ice,R}^{w2i}$, $\psi_{Ice,L}^{i2w}$ and $\psi_{Ice,R}^{i2w}$ have also been solved by a variety of methods, e.g. by the Winer-Hopf method [14] and by the matched eigenfunction expansion method [9].

At infinity, there will be only travelling wave and the velocity potentials above have the following asymptotic forms

$$\psi_k^r = A_k^{\pm} e^{\mp k_0 x} \frac{\cos[k_0(z+H)]}{\cos(k_0 H)} \quad \text{as} \quad x \to \pm\infty \quad (k = 1, 2, 3) \tag{19}$$

$$\psi_0^{s+} = (e^{+k_0 x} + r_0^+ e^{-k_0 x})\frac{\cos[k_0(z+H)]}{\cos(k_0 H)} \quad \text{as} \quad x \to +\infty \tag{20}$$

$$\psi_0^{s+} = t_0^+ e^{+k_0 x} \frac{\cos[k_0(z+H)]}{\cos(k_0 H)} \quad \text{as} \quad x \to -\infty \tag{21}$$

$$\psi_0^{s-} = t_0^- e^{-k_0 x} \frac{\cos[k_0(z+H)]}{\cos(k_0 H)} \quad \text{as} \quad x \to +\infty \tag{22}$$

$$\psi_0^{s-} = (e^{-k_0 x} + r_0^- e^{+k_0 x})\frac{\cos[k_0(z+H)]}{\cos(k_0 H)} \quad \text{as} \quad x \to -\infty \tag{23}$$

$$\psi_{Ice,L}^{w2i} = (e^{+k_0 x} + R_{L,0}^{w2i} e^{-k_0 x})\frac{\cos[k_0(z+H)]}{\cos(k_0 H)} \quad \text{as} \quad x \to +\infty \tag{24}$$

$$\psi_{Ice,L}^{w2i} = T_{L,0}^{w2i} e^{+\kappa_0^{(1)} x} \frac{\cos[\kappa_0^{(1)}(z+H)]}{\cos[\kappa_0^{(1)}(H-d_1)]} \quad \text{as} \quad x \to -\infty \tag{25}$$

$$\psi_{Ice,R}^{w2i} = T_{R,0}^{w2i} \mathrm{e}^{-\kappa_0^{(2)}x} \frac{\cos[\kappa_0^{(2)}(z+H)]}{\cos[\kappa_0^{(2)}(H-d_2)]} \quad \text{as} \quad x \to +\infty \tag{26}$$

$$\psi_{Ice,R}^{w2i} = (\mathrm{e}^{-k_0 x} + R_{R,0}^{w2i} \mathrm{e}^{+k_0 x}) \frac{\cos[k_0(z+H)]}{\cos(k_0 H)} \quad \text{as} \quad x \to -\infty \tag{27}$$

$$\psi_{Ice,L}^{i2w} = T_{L,0}^{i2w} \mathrm{e}^{-k_0 x} \frac{\cos[k_0(z+H)]}{\cos(k_0 H)} \quad \text{as} \quad x \to +\infty \tag{28}$$

$$\psi_{Ice,L}^{i2w} = (\mathrm{e}^{-\kappa_0^{(1)}x} + R_{L,0}^{i2w} \mathrm{e}^{+\kappa_0^{(1)}x}) \frac{\cos[\kappa_0^{(1)}(z+H)]}{\cos[\kappa_0^{(1)}(H-d_1)]} \quad \text{as} \quad x \to -\infty \tag{29}$$

where $A_k^{\pm}$ is the amplitude of radiation potential at $x \to \pm\infty$ due to the forced body oscillation in the *k*-th mode with unit amplitude; $r_0^{\pm}$ and $t_0^{\pm}$ are respectively the reflection and transmission coefficients for the incident wave propagating across the fixed body; $R_{L,0}^{w2i}$ and $R_{R,0}^{w2i}$, $T_{L,0}^{w2i}$ and $T_{R,0}^{w2i}$, are respectively the reflection and transmission coefficients for the incident wave propagating from the open water to the ice covered region; $R_{L,0}^{i2w}$ and $R_{R,0}^{i2w}$, $T_{L,0}^{i2w}$ and $T_{R,0}^{i2w}$, are respectively the reflection and transmission coefficients for the incident wave propagating from the ice covered region to the open water.

With these solutions for the pure wave/body and pure wave/ice interaction problems, we are now able to study the radiation and scattering problems of the body floating on a wide polynya, or the wave/ice/body interaction problem, following the procedure in Srokosz and Evans[28] for the wide spacing multi bodies/wave interaction problem.

C.1 Radiation potential

Here we consider a floating body located at $x = 0$ undergoing oscillation in the *k*-th mode. Near the floating body, we may write the velocity potential as

$$\phi_k(x,z) = \psi_k^r(x,z) + \varepsilon_k^1 \psi_0^{s+}(x,z) + \varepsilon_k^2 \psi_0^{s-}(x,z) \tag{30}$$

Similarly for the ice sheets, noticing that edges are located at $x = x_j$ ($j = 1,2$), we may write the velocity potential as

$$\phi_k(x,z) = \eta_k^1 \psi_{Ice,L}^{w2i}(x - x_1, z) \tag{31}$$

for the left ice sheet and

$$\phi_k(x,z) = \eta_k^2 \psi_{Ice,R}^{w2i}(x - x_2, z) \tag{32}$$

for the right ice sheet.

Here ε_k^1 and ε_k^2, η_k^1 and η_k^2 are unknown coefficients. $x - x_1$ and $x - x_2$ are used respectively in Eqs. (31) and (32) instead of using x, since the ice sheet edge is not situated at the origin $x = 0$, whereas the solutions $\psi_{Ice,L}^{w2i}$ and $\psi_{Ice,R}^{w2i}$ correspond to edge being at the origin.

We may notice that the first term on the right hand side of Eq. (30) is the solution in the absence of the semi-infinite ice sheets. The second and third terms represent the scattering of the wave reflected back from the ice sheets, which are given by Eqs. (20) to (23) based on the large gap assumption. In Eqs. (31) and (32), the right hand sides represent the interaction of propagating wave with semi-infinite ice sheet, with incident potential due to the radiated wave of the body. To determine the unknown coefficients, we choose two vertical interfaces located at $x = x_L$ and $x = x_R$, respectively, as shown in Fig. 1. They are assumed to be sufficiently away from the body and ice edge and the asymptotic formulas in Eqs. (19) to (29) apply. On these two vertical interfaces, the continuous condition of pressure and normal velocity should be enforced, i.e.

$$\phi_k(x_{L-}, z) = \phi_k(x_{L+}, z), \quad \frac{\partial \phi_k(x_{L-}, z)}{\partial x} = \frac{\partial \phi_k(x_{L+}, z)}{\partial x} \tag{33}$$

and

$$\phi_k(x_{R-}, z) = \phi_k(x_{R+}, z), \quad \frac{\partial \phi_k(x_{R-}, z)}{\partial x} = \frac{\partial \phi_k(x_{R+}, z)}{\partial x} \tag{34}$$

where the subscripts + and – mean that the potentials should be taken from the solutions on the left and right hand sides respectively. Substituting the potentials on each side of the interfaces into the above equations, we can have

$$\varepsilon_k^1 = -[(A_k^- t_0^- - A_k^+ r_0^-) R_{L,0}^{w2i} R_{R,0}^{w2i} \mathrm{e}^{k_0(x_1 - x_2)} + A_k^+ R_{R,0}^{w2i} \mathrm{e}^{-k_0(x_1 + x_2)}] / M \tag{35}$$

$$\varepsilon_k^2 = -[(A_k^+ t_0^+ - A_k^- r_0^+) R_{L,0}^{w2i} R_{R,0}^{w2i} \mathrm{e}^{k_0(x_1 - x_2)} + A_k^- R_{L,0}^{w2i} \mathrm{e}^{k_0(x_1 + x_2)}] / M \tag{36}$$

$$\eta_k^1 = -[(A_k^+ t_0^+ - A_k^- r_0^+) R_{R,0}^{w2i} \mathrm{e}^{-k_0 x_2} + A_k^- \mathrm{e}^{k_0 x_2}] / M \tag{37}$$

$$\eta_k^2 = -[(A_k^- t_0^- - A_k^+ r_0^-) R_{L,0}^{w2i} \mathrm{e}^{k_0 x_1} + A_k^+ \mathrm{e}^{-k_0 x_1}] / M \tag{38}$$

where

$$M = (t_0^+ t_0^- - r_0^+ r_0^-) R_{L,0}^{w2i} R_{R,0}^{w2i} \mathrm{e}^{k_0(x_1 - x_2)} - \mathrm{e}^{-k_0(x_1 - x_2)} + r_0^- R_{L,0}^{w2i} \mathrm{e}^{k_0(x_1 + x_2)} + r_0^+ R_{R,0}^{w2i} \mathrm{e}^{-k_0(x_1 + x_2)} \tag{39}$$

Invoking Eq. (30) we can obtain the added mass and damping coefficient for the body floating on polynya from the results for open water, or

$$\mu_{kj} - \mathrm{i}\frac{\lambda_{kj}}{\omega} = \mu_{kj}^{\mathrm{o}} - \mathrm{i}\frac{\lambda_{kj}^{\mathrm{o}}}{\omega} - \varepsilon_j^1 \frac{f_{E,k}^{\mathrm{o}+}}{g} - \varepsilon_j^2 \frac{f_{E,k}^{\mathrm{o}-}}{g} \tag{40}$$

where the superscript o means that the results are from open water, and + and − in $f_{E,k}^{\mathrm{o}}$ mean that the wave exciting force is due to the incident wave opposite to and along *x*-axis respectively. Here the incident wave potential in Eq. (40) is the same as that defined after Eq. (1) with zero ice thickness when computing $f_{E,k}^{\mathrm{o}\pm}$.

From Eqs. (31) and (32), together with Eqs. (25) and (26), we can obtain the asymptotic expressions for the velocity potential ϕ_k

$$\phi_k(x, z) = \eta_k^1 T_{L,0}^{w2i} \mathrm{e}^{+\kappa_0^{(1)}(x - x_1)} \frac{\cos[\kappa_0^{(1)}(z + H)]}{\cos[\kappa_0^{(1)}(H - d_1)]} \quad \text{as} \quad x \to -\infty \tag{41}$$

$$\phi_k(x, z) = \eta_k^2 T_{R,0}^{w2i} \mathrm{e}^{-\kappa_0^{(2)}(x - x_2)} \frac{\cos[\kappa_0^{(2)}(z + H)]}{\cos[\kappa_0^{(2)}(H - d_2)]} \quad \text{as} \quad x \to +\infty \tag{42}$$

Substituting these into the far field formula of Ren *et al.*[25], the damping coefficient can be also written as

$$\lambda_{kj} = \rho\omega[Q_0^{(1)} C_g^{(1)} (\eta_j^1)(\eta_k^1)^* \, |T_{L,0}^{w2i}|^2 + Q_0^{(2)} C_g^{(2)} (\eta_j^2)(\eta_k^2)^* \, |T_{R,0}^{w2i}|^2] \quad (k, j = 1,2,3) \tag{43}$$

where the superscript * denotes complex conjugation,

$$Q_0^{(j)} = \frac{\rho\omega[L_j(\kappa_0^{(j)})^4 + \rho g]}{[L_j(\kappa_0^{(j)})^4 + \rho g - m_j\omega^2]^2} \quad (j = 1, 2) \tag{44}$$

and

$$C_g^{(j)} = \mathrm{i}\frac{\dfrac{\omega}{2\kappa_0^{(j)}}\left(1 + \dfrac{2\kappa_0^{(j)}(H-d_j)}{\sin[2\kappa_0^{(j)}(H-d_j)]}\right) + \dfrac{2L_j(\kappa_0^{(j)})^3\omega}{L_j(\kappa_0^{(j)})^4 + \rho g - m_j\omega^2}}{\dfrac{L_j(\kappa_0^{(j)})^4 + \rho g}{L_j(\kappa_0^{(j)})^4 + \rho g - m_j\omega^2}} \quad (j = 1, 2) \tag{45}$$

is the wave group velocity in the ice covered region.

C.2 Scattering potential

We follow the procedure similar to that used for the radiation above. Near the body, we may write the velocity potential as

$$\phi_0(x,z) = \gamma_1\psi_0^{s+}(x,z) + \gamma_2\psi_0^{s-}(x,z) \tag{46}$$

and near the left and right ice sheets, we may write the velocity potential respectively as

$$\phi_0(x,z) = \psi_{Ice,L}^{i2w}(x - x_1, z) + \beta_1\psi_{Ice,L}^{w2i}(x - x_1, z) \tag{47}$$

$$\phi_0(x,z) = \beta_2\psi_{Ice,R}^{w2i}(x - x_2, z) \tag{48}$$

where γ_1 and γ_2, β_1 and β_2 are constants to be found. The above two equations are based on the assumption that the incident wave is propagating beneath the left ice sheet along the positive direction of x-axis. Substituting Eqs. (19) to (29) into Eqs. (46) to (48) and imposing the matching conditions on $x = x_L$ and on $x = x_R$, we have

$$\gamma_1 = -t_0^- R_{R,0}^{w2i} T_{L,0}^{i2w} \mathrm{e}^{-k_0 x_2} / N \tag{49}$$

$$\gamma_2 = -(\mathrm{e}^{+k_0 x_2} - r_0^+ R_{R,0}^{w2i} \mathrm{e}^{-k_0 x_2}) T_{L,0}^{i2w} / N \tag{50}$$

$$\beta_1 = [-r_0^- \mathrm{e}^{k_0 x_2} + (r_0^- r_0^+ - t_0^- t_0^+) R_{R,0}^{w2i} \mathrm{e}^{-k_0 x_2}] T_{L,0}^{i2w} \mathrm{e}^{+k_0 x_1} / N \tag{51}$$

$$\beta_2 = -t_0^- T_{L,0}^{i2w} / N \tag{52}$$

where

$$N = (t_0^- t_0^+ - r_0^- r_0^+) R_{L,0}^{w2i} R_{R,0}^{w2i} \mathrm{e}^{k_0(x_1 - x_2)} - \mathrm{e}^{-k_0(x_1 - x_2)} + r_0^- R_{L,0}^{w2i} \mathrm{e}^{+k_0(x_1 + x_2)} + r_0^+ R_{R,0}^{w2i} \mathrm{e}^{-k_0(x_1 + x_2)} \tag{53}$$

Invoking Eq. (46) we can obtain the wave exciting force for the body floating on polynya from the results for open water, or

$$f_{E,k} = \gamma_1 f_{E,k}^{o+} + \gamma_2 f_{E,k}^{o-} \tag{54}$$

when Eqs. (12) and (46) are used.

At infinity, the asymptotic form of the velocity potential can be written as

$$\phi(x,z) = \begin{cases} (\mathrm{e}^{-\kappa_0^{(1)}(x - x_1)} + \mathrm{R}\,\mathrm{e}^{\kappa_0^{(1)}(x - x_1)}) \dfrac{\cos[\kappa_0^{(1)}(z+H)]}{\cos[\kappa_0^{(1)}(H - d_1)]}, & x \to -\infty \\ \mathrm{T}\mathrm{e}^{-\kappa_0^{(2)}(x - x_2)} \dfrac{\cos[\kappa_0^{(2)}(z+H)]}{\cos[\kappa_0^{(2)}(H - d_1)]}, & x \to +\infty \end{cases} \tag{55}$$

where R and T are the reflection and transmission coefficients respectively. Then from Eqs. (47) and (48), together with Eqs. (29), (25) and (26) respectively, we have

$$\mathrm{R} = R_{L,0}^{i2w} + \beta_1 T_{L,0}^{w2i} \tag{56}$$

$$\mathrm{T} = \beta_2 T_{R,0}^{w2i} \tag{57}$$

Similar to the damping coefficient, through the asymptotic expressions of Eqs. (55), (41) and (42), the far field equation for the wave exciting force (e.g. Ren *et al.*[25]) gives

$$\begin{aligned} f_{E,k}^{-} &= -2\mathrm{i}\rho g \eta_k^1 T_{L,0}^{w2i} C_g^{(1)} Q_0^{(1)} \\ f_{E,k}^{+} &= -2\mathrm{i}\rho g \eta_k^2 T_{R,0}^{w2i} C_g^{(2)} Q_0^{(2)} \end{aligned} \quad (\, k = 1,2,3 \,) \tag{58}$$

where $Q_0^{(j)}$ and $C_g^{(j)}$ are defined in Eqs. (44) and (45) respectively. Invoking Eqs. (43) and (58), we can obtain the link between the damping coefficient and exciting force as

$$\lambda_{kj} = -\frac{\omega}{4\rho g^2}\left[\frac{1}{C_g^{(1)} Q_0^{(1)}}(f_{E,j}^{-})(f_{E,k}^{-})^* + \frac{1}{C_g^{(2)} Q_0^{(2)}}(f_{E,j}^{+})(f_{E,k}^{+})^*\right] \quad (\, k, j = 1,2,3 \,) \tag{59}$$

It is noticeable that the identity above is the same as Eq. (47) in Li *et al.*[32] obtained from the exact solution.

III. NUMERICAL RESULTS

We shall first demonstrate the accuracy and efficiency of the present method. This is to be achieved by comparing the obtained results with the ‘exact’ solution. After the method is verified, we shall use the formulation to provide some insights into the features of the hydrodynamic force and body motion, in particular its highly oscillatory behaviour. The numerical results are presented in the nondimensionalized form, based on a characteristic length scale, the density of water ρ and acceleration due to gravity g.

A. Wave propagation across a polynya

We first consider the case for a wave propagating underneath the left ice sheet. It passes through a polynya and moves into the right ice sheets. As the body is removed, the wide polynya approximation is made on the basis that its width is much larger than the wavelength. Then the reflection and transmission coefficients can be obtained directly by letting $r_0^+ = r_0^- = 0$, $t_0^+ = t_0^- = 1$ in Eqs. (56) and (57), or

$$\mathrm{R} = R_{L,0}^{i2w} + \frac{R_{R,0}^{w2i} T_{L,0}^{i2w} T_{L,0}^{w2i} \mathrm{e}^{-2k_0(x_2 - x_1)}}{1 - R_{L,0}^{w2i} R_{R,0}^{w2i} \mathrm{e}^{-2k_0(x_2 - x_1)}} \tag{60}$$

$$\mathrm{T} = \frac{T_{L,0}^{i2w} T_{R,0}^{w2i} \mathrm{e}^{-k_0(x_2 - x_1)}}{1 - R_{L,0}^{w2i} R_{R,0}^{w2i} \mathrm{e}^{-2k_0(x_2 - x_1)}} \tag{61}$$

which can be found to satisfy the energy conservation equation (i.e. Eq. (A2) in Ren *et al.*[25]). These two equations may also be obtained by using the procedure in Meylan and Squire[33] for wave propagation across a finite floe. Assume that the incoming wave is from $x = -\infty$. Near the left ice sheet edge at $x = x_1$, if we ignore the evanescent waves, we can consider the two travelling waves with complex amplitudes w_a and w_b, propagating along and opposite to *x*-axis, respectively. The reflection coefficient R at $x=-\infty$ should be due to the reflection (semi-infinite ice to semi-infinite free surface) and transmission of w_b (semi-infinite water to semi-infinite ice). Thus

$$\mathrm{R} = R_{L,0}^{i2w} + w_b T_{L,0}^{w2i} \tag{62}$$

On the other hand, w_a is due to the combination of transmission (semi-infinite ice to semi-infinite water) and reflection of w_b (semi-infinite water to semi-infinite ice),

$$w_a = T_{L,0}^{i2w} + w_b R_{L,0}^{w2i} \tag{63}$$

At the other ice sheet edge $x = x_2$, the waves of w_a and w_b should have a phase shift

$$w_a \mathrm{e}^{-k_0(x-x_1)} = w_a \mathrm{e}^{-k_0(x_2-x_1)} \mathrm{e}^{-k_0(x-x_2)} \tag{64}$$

$$w_b \mathrm{e}^{k_0(x-x_1)} = w_b \mathrm{e}^{k_0(x_2-x_1)} \mathrm{e}^{k_0(x-x_2)} \tag{65}$$

which means that their complex amplitudes at $x = x_2$ become $w_a \mathrm{e}^{-k_0(x_2-x_1)}$ and $w_b \mathrm{e}^{k_0(x_2-x_1)}$, respectively. Then $w_b \mathrm{e}^{k_0(x_2-x_1)}$ is due to the reflection of $w_a \mathrm{e}^{-k_0(x_2-x_1)}$ (semi-infinite water to semi-infinite ice),

$$w_b \mathrm{e}^{k_0(x_2-x_1)} = w_a \mathrm{e}^{-k_0(x_2-x_1)} R_{R,0}^{w2i} \tag{66}$$

and the wave at $x = +\infty$ is due to the transmission of $w_a \mathrm{e}^{-k_0(x_2-x_1)}$

$$\mathrm{T} = w_a \mathrm{e}^{-k_0(x_2-x_1)} T_{R,0}^{w2i} \tag{67}$$

From Eqs. (63) and (66), we have

$$w_a = \frac{T_{L,0}^{i2w}}{1 - R_{R,0}^{w2i} R_{L,0}^{w2i} \mathrm{e}^{-2k_0(x_2-x_1)}} \tag{68}$$

$$w_b = \frac{T_{L,0}^{i2w} R_{R,0}^{w2i} \mathrm{e}^{-2k_0(x_2-x_1)}}{1 - R_{R,0}^{w2i} R_{L,0}^{w2i} \mathrm{e}^{-2k_0(x_2-x_1)}} \tag{69}$$

Substituting Eqs. (69) and (68) into Eqs. (62) and (67), we can further obtain the expression for R and T, which are identical to Eqs. (60) and (61). Therefore for this particular case the procedure in Meylan and Squire[33] and the present method give the same result. It also ought to point out that in Meylan and Squire[33] the origin was taken at one of the edges, while here in Eqs. (47) and (48), the origin is taken at $x = x_1$ and x_2 respectively.

The reflection and transmission coefficients between semi-infinite $i2w$ (ice to water) and semi-infinite $w2i$ (water to ice) are in fact related. Similar to Meylan and Squire[33], we may use Stokes time reverse and obtain

$$R_{L,0}^{i2w} = -\frac{(R_{L,0}^{w2i})^* T_{L,0}^{w2i}}{(T_{L,0}^{w2i})^*}, \quad T_{L,0}^{i2w} = \frac{1 - |R_{L,0}^{w2i}|^2}{(T_{L,0}^{w2i})^*} \tag{70}$$

which can also be obtained by using the Green identity, for example Eq. (A1) in Ren *et al.*[25] through replacing ϕ and ϕ^* by ϕ^{i2w} and $(\phi^{w2i})^*$, then by ϕ^{i2w} and ϕ^{w2i}, and by ϕ^{w2i} and $(\phi^{w2i})^*$.

To verify the accuracy and efficiency of the present method, we consider the polynya with the following parameters

$$H = 5\,,\quad h_2 = h_1 = 0.02\,,\quad m_2 = m_1 = 0.018\,,\quad L_2 = L_1 = 0.003647 \tag{71}$$

The characteristic length scale above has been chosen as the polynya width $l = x_2 - x_1$. Fig. 2 and Fig. 3 show the reflection and transmission coefficients at zero ice draught and at $d_2 = d_1 = 0.018$, respectively, against $|k_0 l|$. It can be seen from these two figures that the present numerical results agree very well with those exact solutions which are calculated through the eigenfunction method in Ren *et al.*[25]. Strictly speaking, the present approximation should be valid only when the width is much larger than the wavelength, or $|k_0 l| >> 1$. However, it can be seen from Eqs. (60) and (61) that $|\mathrm{R}| \to 0$ and $|\mathrm{T}| \to 1$ when $|k_0 l| \to 0$, which is in fact a result of the exact solution [16]. Thus it is not a total surprise that the present approximate method can give such an accurate result for the whole wave frequency span shown in Fig. 2 and Fig. 3.

From the exact solution of Chung and Linton[16] for zero ice draught, it was found that there was an infinite number of discrete frequencies at which the reflection coefficient R could be zero. Here when the left and right ice sheets have the same physical properties, we have $R = R_{R,0}^{w2i} = R_{L,0}^{w2i}$, $T = T_{R,0}^{w2i} = T_{L,0}^{w2i}$. The substitution of Eq. (70) into Eq. (60) provides

$$\mathrm{R} = -\frac{T}{T^* R} S_{\mathrm{R}}(\omega) \tag{72}$$

where

$$S_{\mathrm{R}}(\omega) = \frac{\mathrm{e}^{2\mathrm{i}(\delta+\beta)} - 1}{\mathrm{e}^{2\mathrm{i}(\delta+\beta)} - 1/|R|^2} \tag{73}$$

with $\delta = \mathrm{i}k_0 l$ and $\beta = \mathrm{Arg}(R) \in [0, 2\pi)$ which is the argument of R. Eq. (73) maps the unit circle $\mathrm{e}^{2\mathrm{i}(\delta+\beta)}$ to a circle with centre at $1/(1+1/|R|^2)$ and radius of $1/(1+1/|R|^2)$, from which we find that $|\mathrm{R}|$ will reach its troughs (i.e. zero) when δ equals

$$\delta_T^{\mathrm{R}} = n\pi - \beta \tag{74}$$

and will reach its peaks when δ equals

$$\delta_P^{\mathrm{R}} = n\pi + \pi/2 - \beta \tag{75}$$

where n includes all integers which ensure $\delta < 0$ required based on the definition of k_0. This can be seen in Fig. 2 at zero ice draught. These two equations can be further explained by the physical process of the wave motion in the polynya. From Eq. (70) the phase of the first term on the right hand side of Eq. (62) can be obtained as

$$\mathrm{Arg}(R_{L,0}^{i2w}) = -\beta + 2\gamma + \pi \tag{76}$$

where $\gamma = \mathrm{Arg}(T)$. When the incoming wave passes through the ice sheet edge at $x = x_1$, the transmitted wave can be written as

$$w_1 = T_{L,0}^{i2w} \mathrm{e}^{-k_0(x-x_1)} \tag{77}$$

When w_1 reaches the right ice sheet edge at $x = x_2$, there will be a reflected wave

$$w_2 = T_{L,0}^{i2w} R \mathrm{e}^{-k_0 l} \mathrm{e}^{k_0(x-x_2)} \tag{78}$$

When w_2 reaches the left ice sheet edge at $x = x_1$, there will be a transmitted wave into the ice sheet

$$w_3 = T_{L,0}^{i2w} R T \mathrm{e}^{-2k_0 l} \mathrm{e}^{\kappa_0^{(1)}(x-x_1)} \tag{79}$$

The phase of the complex amplitude of this wave is then equal to $\beta + 2\gamma + 2\delta$ (note that we have $\mathrm{Arg}(T_{L,0}^{i2w}) = \mathrm{Arg}(T_{L,0}^{w2i})$ according to the second equation in Eq. (70)). Its difference with the phase in Eq. (76) is then $2\beta + 2\delta - \pi$. When this is equal to $2n\pi + \pi$, Eq. (79) will be out of phase with the reflected wave in the first term of Eq. (62) and the combined wave will be reduced. Similarly when the difference is equal to $2n\pi$, the combined wave will increase. This is consistent with Eqs. (74) and (75).

In addition to the reflection and transmission coefficients R and T, we further investigate the accuracy of the present method for the local wave, through the wave elevation in polynya obtained from

$$\frac{\eta_0}{\alpha_0} = -\frac{\mathrm{i}\omega}{g}\phi_0(x,0) \tag{80}$$

Three points are chosen and they are respectively taken at the edge of left ice sheet $x = x_1$, middle in the open water $x = (x_1 + x_2)/2$, and the edge of right ice sheet $x = x_2$. The wave elevations are shown in Fig. 4. It can be seen that the results from the present method almost coincide with the exact solution, which shows the approximate method can give a very accurate result for the local wave across the frequency range.

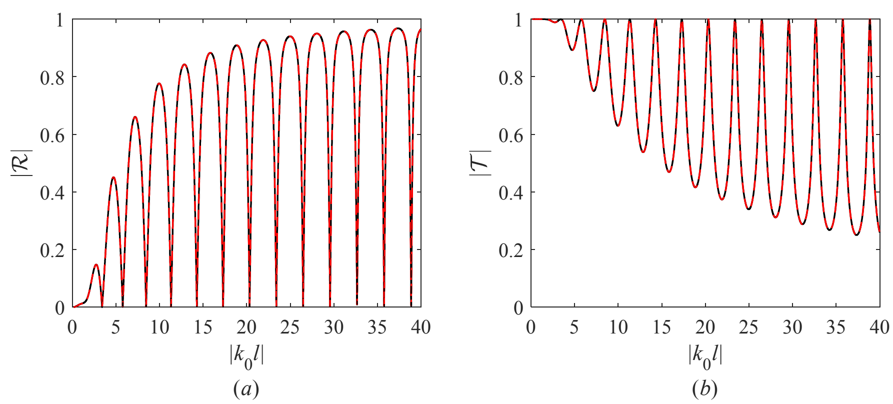

Fig. 2. Reflection and transmission coefficients for a wave propagating across a polynya with zero ice draught. (*a*) reflection coefficient; (*b*) transmission coefficient. Solid lines: exact results computed by the matched eigenfunction expansions in Ren *et al.*[25]; dashed lines: computed by formula Eqs. (60) and (61). ($H = 5$, $x_1 = -x_2 = -0.5$, $h_2 = h_1 = 0.02$, $d_2 = d_1 = 0$, $m_2 = m_1 = 0.018$, $L_2 = L_1 = 0.003647$)

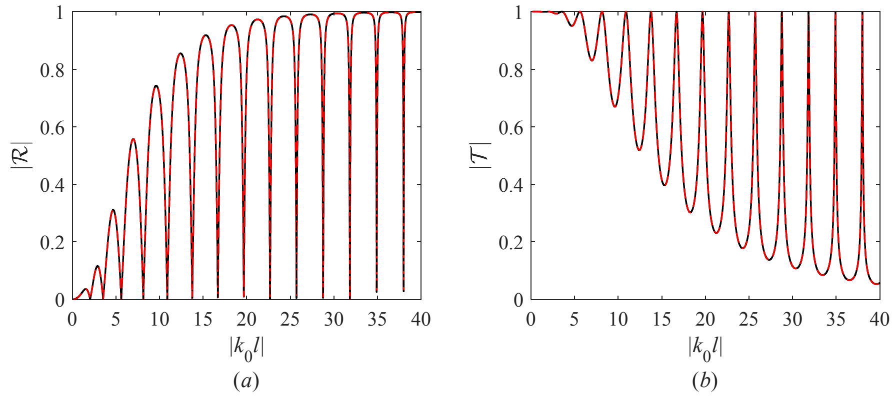

Fig. 3. Reflection and transmission coefficients for a wave propagating across a polynya with nonzero ice draught. (*a*) reflection coefficient; (*b*) transmission coefficient. Solid lines: exact results computed by the matched eigenfunction expansions in Ren *et al.*[25]; dashed lines: computed by formula Eqs. (60) and (61). ($H = 5$, $x_1 = -x_2 = -0.5$, $h_2 = h_1 = 0.02$, $d_2 = d_1 = 0.018$, $m_2 = m_1 = 0.018$, $L_2 = L_1 = 0.003647$)

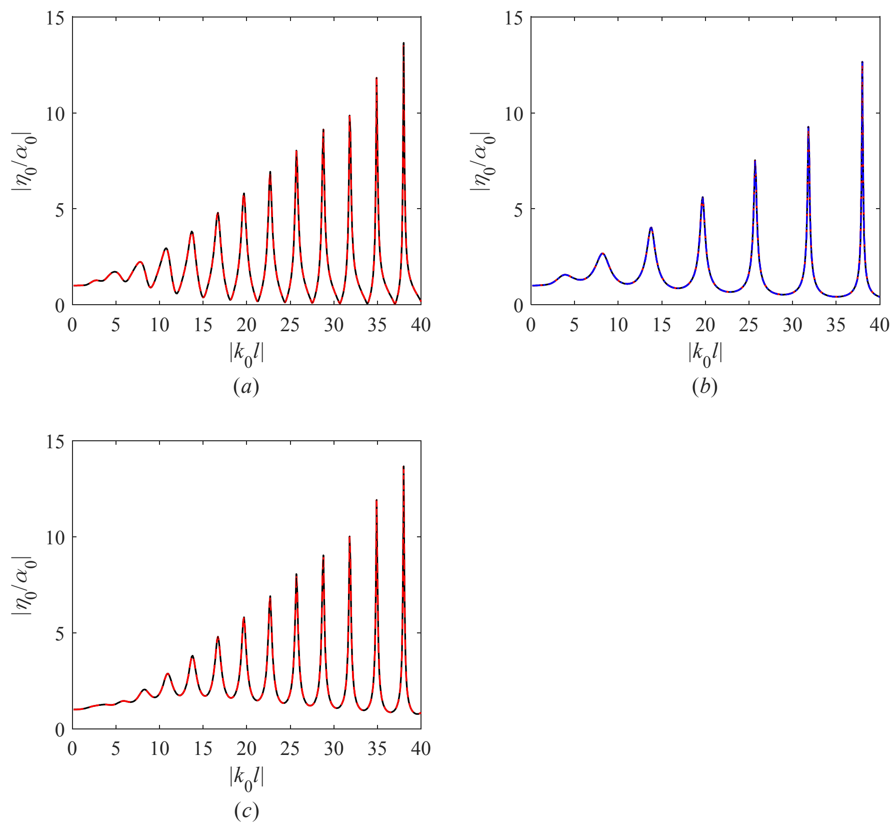

Fig. 4. Wave elevation at different location in polynya. (*a*) $x = x_1$; (*b*) $x = (x_1 + x_2)/2$. (*c*) $x = x_2$. Solid lines: exact results computed by the matched eigenfunction expansions in Ren *et al.*[25]; dashed lines: results computed by formula Eq. (47) for $x < 0$ and Eq. (48) for $x > 0$. In figure (*b*), the dashed line is by Eq. (47), while the

dashed-dotted line is by Eq. (48). ($H = 5$, $x_1 = -x_2 = -0.5$, $h_2 = h_1 = 0.02$, $d_2 = d_1 = 0.018$, $m_2 = m_1 = 0.018$, $L_2 = L_1 = 0.003647$)

B. Wave interaction with a submerged ellipse

The case chosen for further comparison is an elliptic cylinder defined as $(x - x_0)^2 / a^2 + (z - z_0)^2 / b^2 = 1$, where a and b are its half axes in x and z directions, respectively, and (x_0, z_0) is the centre of the cylinder, at which the rotational centre is located, or $(x', z') = (x_0, z_0)$. The characteristic length scale is chosen as a . The exact solution for this problem has been obtained by the source distribution method [24] using the Green function satisfying all the boundary conditions apart from that on the body surface. Here we use the hybrid method [27]. Fig. 5 and Fig. 6 respectively show the added mass and damping coefficient against the nondimensional wave number in deep open water or $\sigma = a\omega^2 / g$, while Fig. 7 presents the corresponding wave exciting force. The parameters are chosen as the same as those in Sturova[24]. These figures show that there is no real visible difference between the results obtained from the present method and the exact solution. The damping coefficient and exciting force are also computed by the far field formula and obtained results virtually coincide with those from the near field formula. We may notice that the width of the polynya is only two and half times the body width. The excellent agreement across the frequency span shows the effectiveness of present method, even though it is based on the large gap assumption.

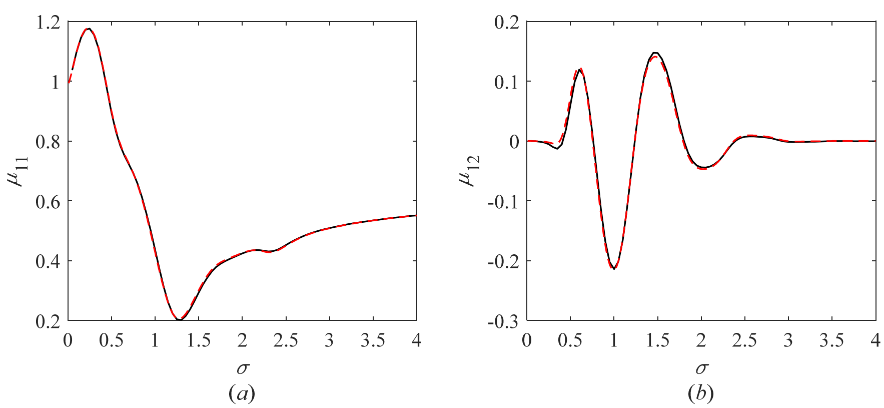

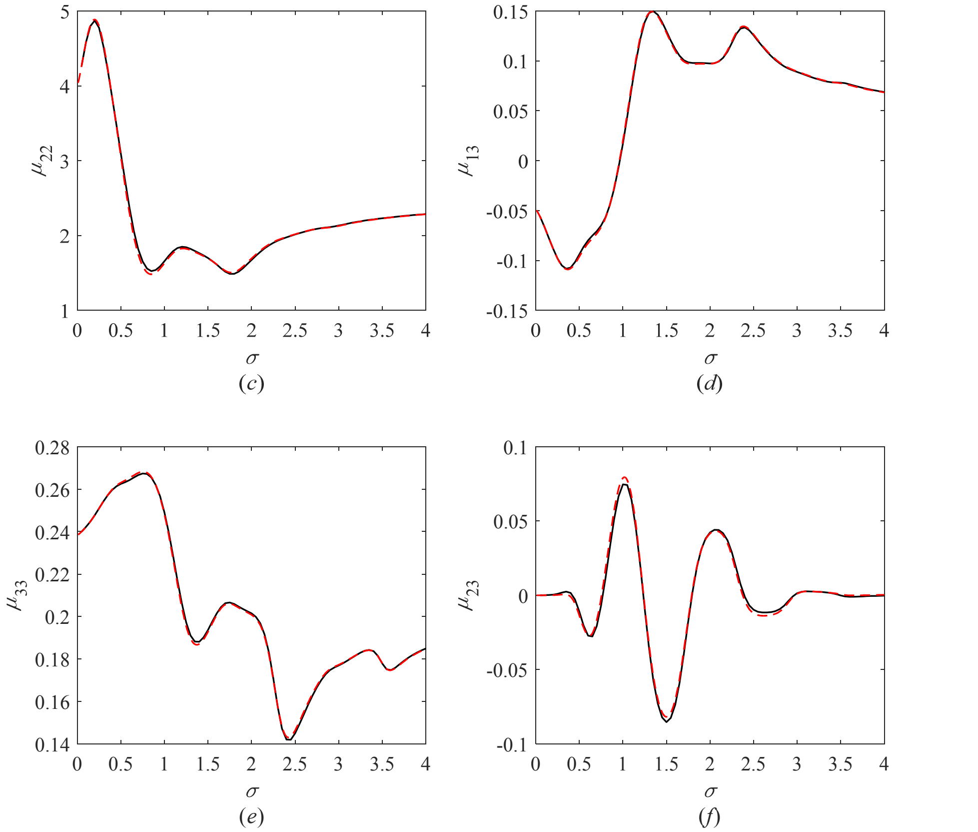

Fig. 5. Added mass of a submerged elliptic cylinder. (*a*) sway; (*b*) sway-heave; (*c*) heave; (*d*) sway-roll; (*e*) roll; (*f*) heave-roll. Solid lines: results computed by the hybrid method in Li *et al.*[27]; dashed lines: results computed by the present method. ($a=1$, $b=0.5$, $(x',z')=(0,-1)$, $H=25$, $x_1=-x_2=-2.5$, $h_1=0.025$ and $h_2=0.1$, $d_1=0$ and $d_2=0$, $m_1=0.0225$ and $m_2=0.09$, $L_1=0.0356$ and $L_2=2.2791$)

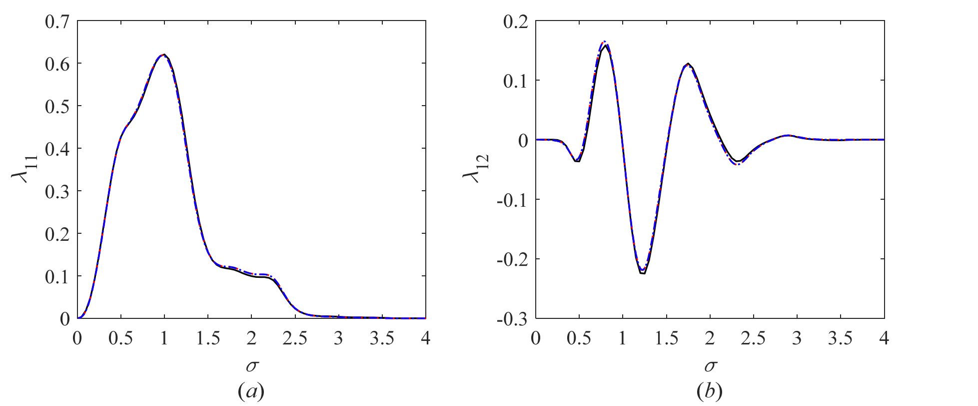

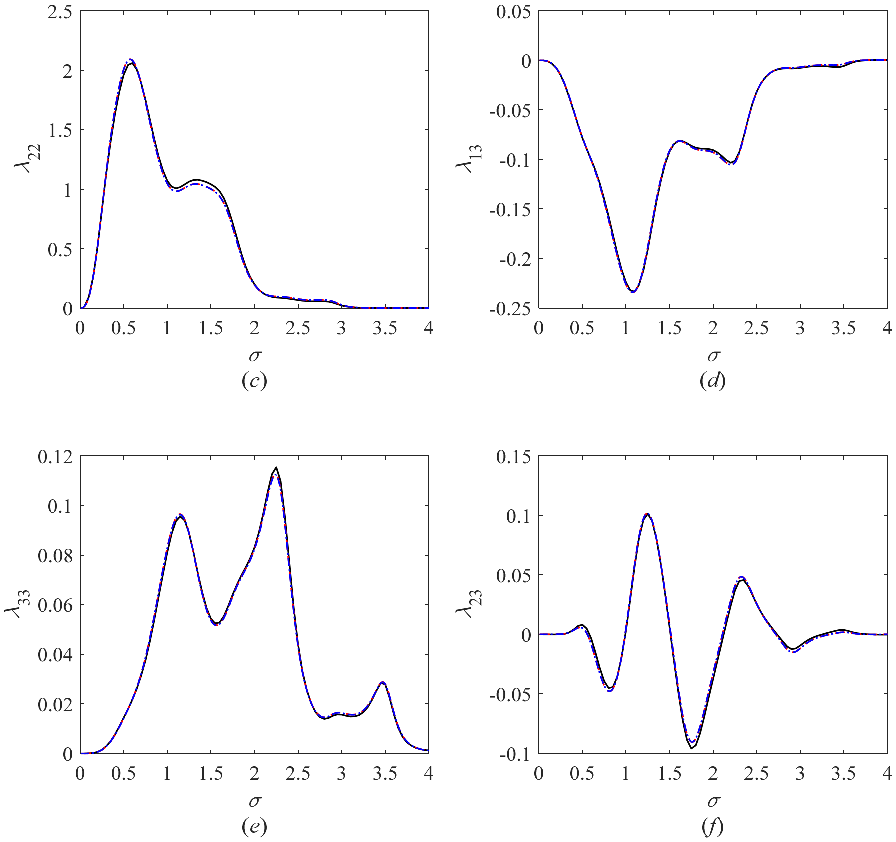

Fig. 6. Damping coefficient of an elliptical cylinder. (*a*) sway; (*b*) sway-heave; (*c*) heave; (*d*) sway-roll; (*e*) roll; (*f*) heave-roll. Solid lines: results computed by the hybrid method in Li *et al.*[27]; dashed lines: results computed by the present method; dash-dotted lines: same to dashed lines, but by the far field formula. ($a=1$, $b=0.5$, $(x',z')=(0,-1)$, $H=25$, $x_1=-x_2=-2.5$, $h_1=0.025$ and $h_2=0.1$, $d_1=0$ and $d_2=0$, $m_1=0.0225$ and $m_2=0.09$, $L_1=0.0356$ and $L_2=2.2791$)

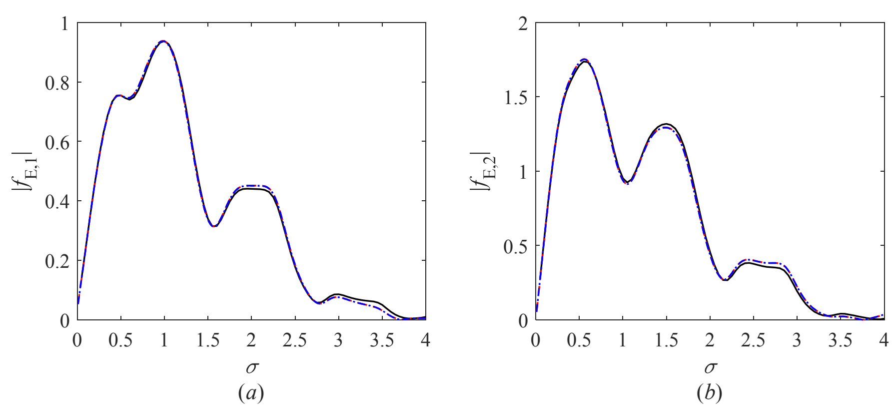

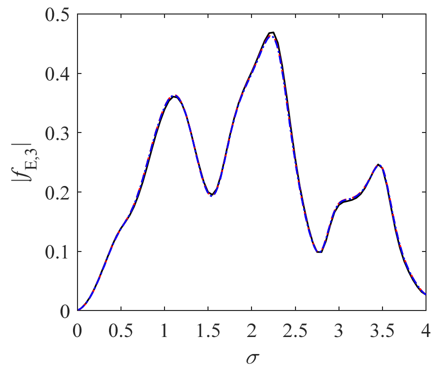

(*c*)

Fig. 7. Wave exciting force on an elliptical cylinder. (*a*) sway; (*b*) heave; (*c*) roll. Solid lines: results computed by the hybrid method in Li *et al.*[27]; dashed lines: results computed by the present method; dash-dotted lines: same to dashed lines, but by the far field formula. ($a=1$, $b=0.5$, $(x',z')=(0,-1)$, $H=25$, $x_1=-x_2=-2.5$, $h_1=0.025$ and $h_2=0.1$, $d_1=0$ and $d_2=0$, $m_1=0.0225$ and $m_2=0.09$, $L_1=0.0356$ and $L_2=2.2791$)

C. Wave interaction with a floating rectangle body

The case chosen now is a floating rectangle body, and it is beam a is taken as the characteristic length scale. The added mass and damping coefficient for the floating rectangle body against $\sigma = a\omega^2/g$ are respectively shown in Fig. 8 and Fig. 9, while the corresponding wave exciting force is presented in Fig. 10. From these figures we can see that once again there is no visible difference between the results from the present method and the exact solution using the eigenfunction method [25]. It can be seen from Fig. 3 of Ren *et al.*[25] that the radiation force for the body respectively floating on the polynya and open water tend to the same value at very small σ (noticing that they will be slightly different from that with an ice sheet of non-zero draught). It can also be seen from Fig. 3 that the reflection and transmission coefficients for the wave/semi-infinite ice sheet interaction problem will respectively tend to 0 and 1 for very long waves. As $\sigma \to 0$, from Eq. (40) both coefficients ε_j^1 and ε_j^2 will tend to 0, and from Eq. (54) the coefficients γ_1 and γ_2 will respectively tend to 0 and 1 (noticing that there is a phase difference $-k_0 x_1$ in the definition of incident potential when computing the exciting force). These are the same as those from the exact solution. Then the hydrodynamic force computed by the present method will tend to that in open water for very long wave, i.e. tend to the exact solution with ice draught effect ignored.

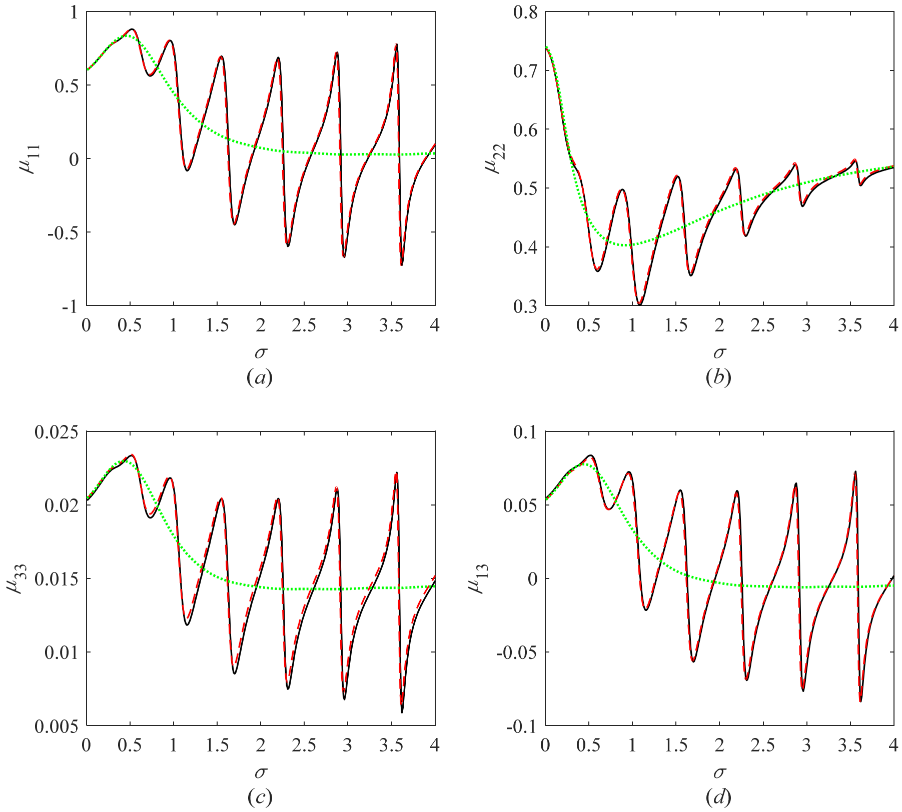

Fig. 8. Added mass of a floating rectangular body. (*a*) sway; (*b*) heave; (*c*) roll; (*d*) sway-roll or roll-sway. Solid lines: semi-analytical solution in Ren *et al.*[25]; dashed lines: results computed by the present method; dotted lines: results for open water. ($a=1$, $b=0.5$, $(x',z')=(0,-b/2)$, $H=10$, $x_1=-x_2=-5$, $h_1=h_2=0.1$, $d_1=d_2=0.09$, $m_1=m_2=0.09$, $L_1=L_2=4.5582$)

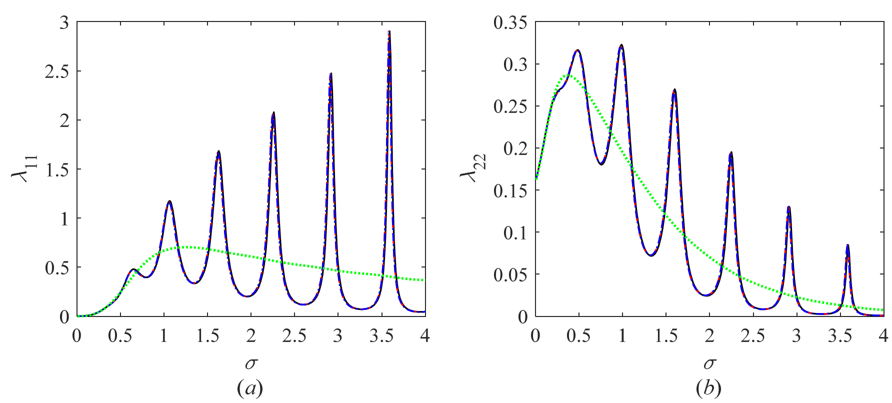

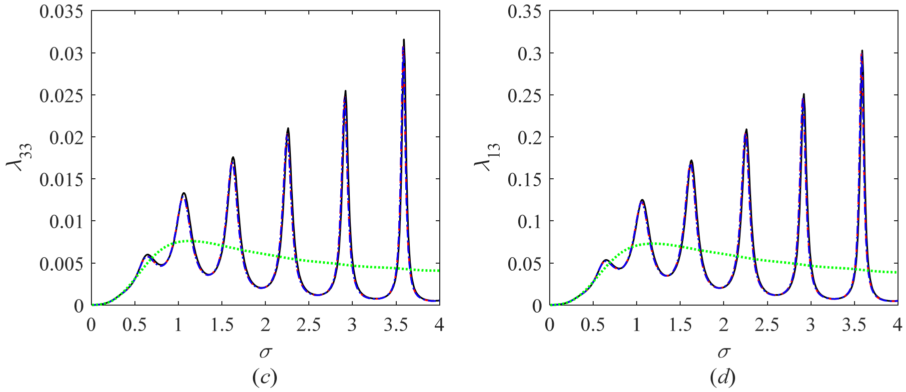

Fig. 9. Damping coefficient of a floating rectangular body. (*a*) sway; (*b*) heave; (*c*) roll; (*d*) sway-roll or roll-sway. Solid lines: semi-analytical solution in Ren *et al.*[25]; dashed lines: results computed by the present method; dash-dotted lines: same to dashed lines, but by the far field formula; dotted lines: results for open water. ($a=1$, $b=0.5$, $(x',z')=(0,-b/2)$, $H=10$, $x_1=-x_2=-5$, $h_1=h_2=0.1$, $d_1=d_2=0.09$, $m_1=m_2=0.09$, $L_1=L_2=4.5582$)

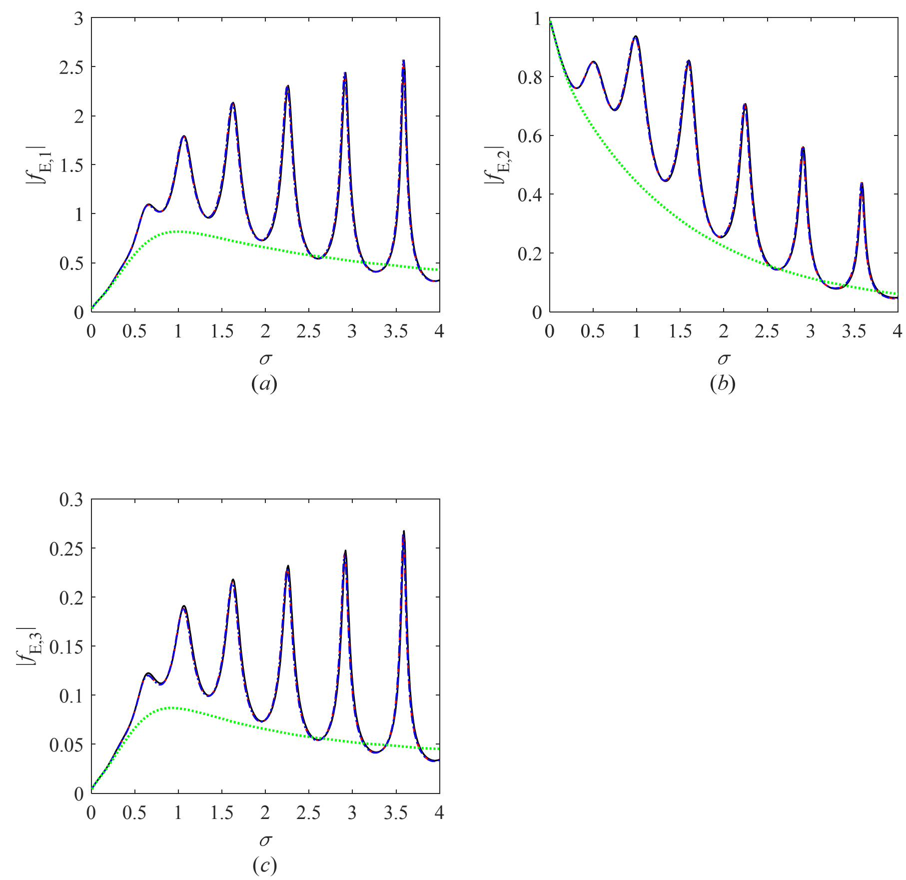

Fig. 10. Wave exciting force on a floating rectangular body. (*a*) sway; (*b*) heave; (*c*) roll. Solid lines:

semi-analytical solution in Ren *et al.*[25]; dashed lines: results computed by the present method; dash-dotted lines: same to dashed lines, but by the far field formula; dotted lines: results for open water. ($a = 1$, $b = 0.5$, $(x', z') = (0, -b/2)$, $H = 10$, $x_1 = -x_2 = -5$, $h_1 = h_2 = 0.1$, $d_1 = d_2 = 0.09$, $m_1 = m_2 = 0.09$, $L_1 = L_2 = 4.5582$)

We then investigate the accuracy of the wide spacing approximation through varying the gap width between the ice edge and the body. Heave mode is taken as an example. The added mass and damping coefficient are presented in Fig. 11, against $\ell = \ell_1 = \ell_2$, where $\ell_1 = |x_1 + a/2|$ and $\ell_2 = |x_2 - a/2|$. At $\sigma = 1.0$, the results are almost the same as those from the exact solution even when the ice edge nearly touches the body. The difference begins to appear when $\ell < 1.0$ for the cases of $\sigma = 2.0$ and $\sigma = 3.0$. We have already discussed previously that the result from the present method tends to the exact solution as $\sigma \to 0$ for any ℓ . Also at very high frequencies, all the evanescent modes decay rapidly. These with Fig. 11 show that there will be some noticeable difference between the result of wide spacing approximation and the exact solution only when the gap between the ice edge and body is very small and the frequency is within certain range.

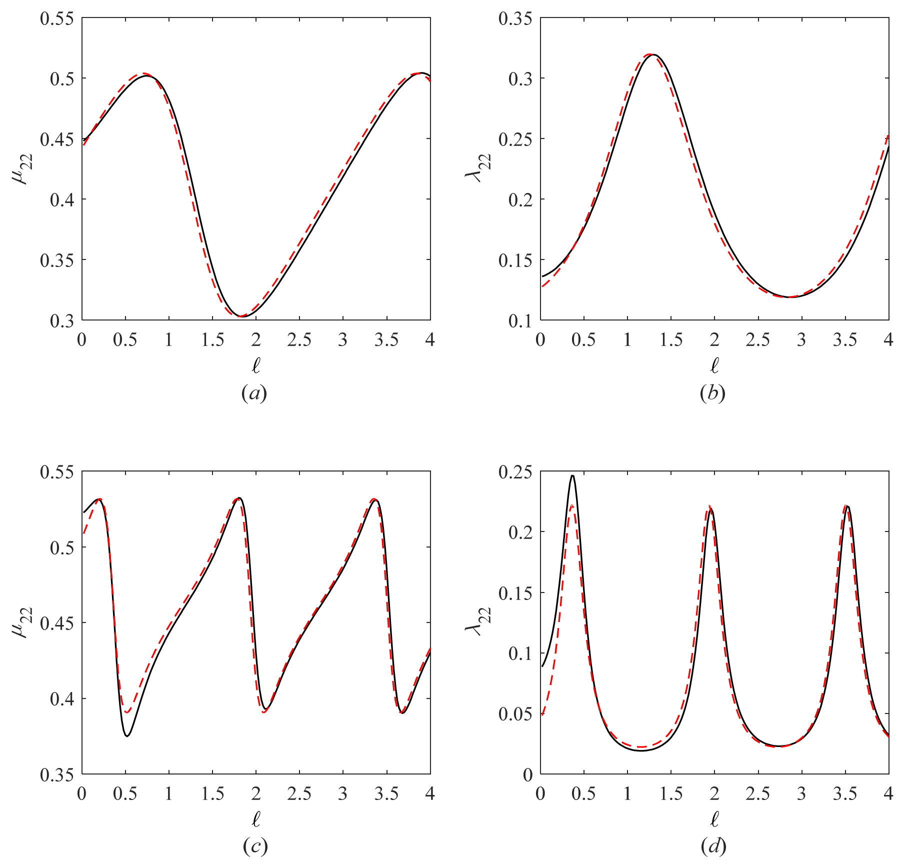

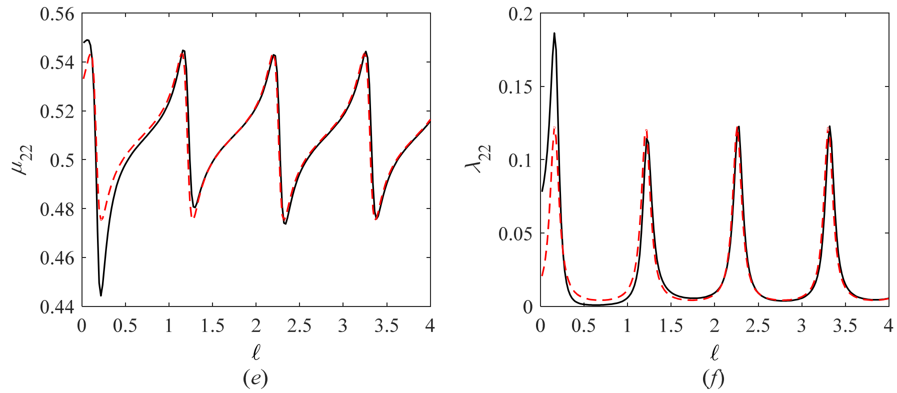

Fig. 11. Hydrodynamic coefficients of a floating rectangular body in heave mode. In (*a*) and (*b*), $\sigma = 1.0$; In (*c*) and (*d*), $\sigma = 2.0$; in (*e*) and (*f*), $\sigma = 3.0$. Solid lines: results computed by the exact method; dashed lines: results computed by the present method. ($a = 1$, $b = 0.5$, $(x', z') = (0, -b/2)$, $H = 10$, $h_1 = h_2 = 0.1$, $d_1 = d_2 = 0.09$, $m_1 = m_2 = 0.09$, $L_1 = L_2 = 4.5582$)

D. Oscillatory features of the hydrodynamic force and body motion

The above comparisons show that the present method, based on the wide polynya assumption, is accurate and efficient for a body in polynya across the frequency span. This allows us to use the explicit form of the derived formula to give some insights into the behaviours of the hydrodynamic force and body motion.

D.1 Oscillation features of the hydrodynamic force

Highly oscillatory behaviour of the hydrodynamic force has been observed in the wave/body/ice interaction problems [25], which is different from the typical case of a body floating on open water. From Eqs. (40) and (54), we can see that the oscillatory behaviour of the hydrodynamic force is closely linked to the coefficients ε_j^1 and ε_j^2 , γ_1 and γ_2 . If we look Eq. (30) carefully, we may see that the right hand side terms related to ε_j^1 and ε_j^2 are due to the refection of the body generated wave by the ice sheet. The reflected wave will then be reflected back by the body to ice sheet, which will be further reflected back to the body by the ice sheet. This resembles the sloshing wave inside a tank in which the waves continue to be reflected by the side walls, leading to the oscillatory behaviour.

We may use the case in section C as an example. Due to symmetry of the problem, we have $\varepsilon_j^1 = (-1)^j \varepsilon_j^2$ and $f_{E,k}^{\mathrm{o}+} = (-1)^k f_{E,k}^{\mathrm{o}-}$. The coefficients ε_j^2 in Eq. (36) can be written as

$$\varepsilon_j^2 = -\frac{(A_j^+ t_0^+ - A_j^- r_0^+) R_{L,0}^{w2i} R_{R,0}^{w2i} \mathrm{e}^{-k_0 l} + A_j^- R_{L,0}^{w2i}}{(t_0^+ t_0^- - r_0^+ r_0^-) R_{L,0}^{w2i} R_{R,0}^{w2i} \mathrm{e}^{-k_0 l} - \mathrm{e}^{k_0 l} + r_0^- R_{L,0}^{w2i} + r_0^+ R_{R,0}^{w2i}} \tag{81}$$

where $l = 2x_2 = -2x_1$. It is well known that with the increase of σ , we have $t_0^+ = t_0^- \to 0$. Thus for relatively large σ , by letting $t_0^+ = t_0^- = 0$ Eq. (81) can be simplified as

$$\varepsilon_j^2 = \frac{A_j^- R}{\mathrm{e}^{k_0 l} - rR} \tag{82}$$

where $r = r_0^+ = r_0^-$. Then invoking Eq. (82) we can find the peaks and troughs of $|\varepsilon_j^2|$ through

$$|S_\varepsilon(\omega)| = |\mathrm{e}^{k_0 l} - rR| = \sqrt{1 + |rR|^2 - 2\,\mathrm{Re}(rR\mathrm{e}^{-k_0 l})} \tag{83}$$

It shows that $|\varepsilon_j^2|$ will reach its peaks when $\delta = \mathrm{i}k_0 l$ equals

$$\delta_P^\varepsilon = 2n\pi - \beta - \mathrm{Arg}(r) \tag{84}$$

and reach its troughs when δ equals

$$\delta_T^\varepsilon = 2n\pi + \pi - \beta - \mathrm{Arg}(r) \tag{85}$$

where n includes all integers which ensure $\delta < 0$ required based on the definition of k_0. From Eq. (58), the far field formula for $f_{E,k}^{\mathrm{o}-}$ can be given as

$$f_{E,k}^{\mathrm{o}-} = -2\mathrm{i}\rho\omega A_k^- C_g \tag{86}$$

where C_g is the wave group velocity in the open water. Substituting Eqs. (82) and (86) into Eq. (40), we have

$$\mu_{kj} = \mu_{kj}^{\mathrm{o}} - \frac{2\rho\omega C_g[1 + (-1)^{j+k}]}{g}\mathrm{Im}(A_{kj}) \tag{87}$$

$$\lambda_{kj} = \lambda_{kj}^{\mathrm{o}} - \frac{2\rho\omega^2 C_g[1 + (-1)^{j+k}]}{g}\mathrm{Re}(A_{kj}) \tag{88}$$

where

$$A_{kj} = \frac{A_j^- A_k^- R}{\mathrm{e}^{k_0 l} - rR} \tag{89}$$

The denominator of this equation is the same as that of Eq. (82) and therefore Eqs. (84) and (85) apply here. From Eqs. (8.6.26) and (8.6.49) of Mei *et al.*[29], we have

$$\mathrm{Arg}(r) = \mathrm{Arg}(t_0^-) + \pi/2 \tag{90}$$

and

$$r + (-1)^j t_0^- = -\mathrm{e}^{2\mathrm{i}\mathrm{Arg}(A_j^-)} \tag{91}$$

Thus when $\delta = \delta_P^\varepsilon$ in Eq. (84) we have

$$A_{kj} = \frac{|A_j^- A_k^- R|}{1 - |rR|}\mathrm{e}^{\mathrm{i}[\mathrm{Arg}(A_j^-) + \mathrm{Arg}(A_k^-) - \mathrm{Arg}(r)]} = \begin{cases} -\dfrac{|A_j^- A_k^- R|}{1 - |rR|}[|r| + \mathrm{i}|t_0^-|], & j,k = 1,3 \\ -\dfrac{|A_j^- A_k^- R|}{1 - |rR|}[|r| - \mathrm{i}|t_0^-|], & j,k = 2 \end{cases} \tag{92}$$

while when $\delta = \delta_T^\varepsilon$ in Eq. (85) we have

$$A_{kj} = -\frac{|A_j^- A_k^- R|}{1 + |rR|}\mathrm{e}^{\mathrm{i}[\mathrm{Arg}(A_j^-) + \mathrm{Arg}(A_k^-) - \mathrm{Arg}(r)]} = \begin{cases} \dfrac{|A_j^- A_k^- R|}{1 + |rR|}[|r| + \mathrm{i}|t_0^-|], & j,k = 1,3 \\ \dfrac{|A_j^- A_k^- R|}{1 + |rR|}[|r| - \mathrm{i}|t_0^-|], & j,k = 2 \end{cases} \tag{93}$$

It should be noticed that $t_0^+ = t_0^- \to 0$ has been used for a large σ, in Eqs. (84) and (85) and it may be used in Eqs. (92) and (93) as well. Therefore, when, λ_{kj} will reach its peaks and troughs at $\delta = \delta_P^\varepsilon$ and $\delta = \delta_T^\varepsilon$ respectively, μ_{kj} will reach the value of μ_{kj}^{o}, or the last term in Eq. (87)

due to ice sheet has no effect. These results can be seen in Fig. 12. We should also notice that Eqs. (87) and (88) are for a body of symmetry. $\mu_{kj}=0$ and $\lambda_{kj}=0$ when $k+j$ is an odd number, and therefore only even $k+j$ is discussed.

Invoking Eq. (40), we can see that the hydrodynamic coefficients will follow the oscillatory behaviour of ε_j^2 and the oscillation period in terms of $|k_0 l|$ roughly equals 2π. This is reflected in Fig. 12, but the period of 2π is not exact as other parameters in Eq. (81) vary with σ or k_0 when l is fixed. Thus in Fig. 13, results are plotted against $|k_0 l|$ at various given σ while varying l. From the figure, it can be seen that the period is 2π, as expected from Eq. (81).

For the wave exciting force, Eq. (54) can be rewritten as

$$f_{E,k}=\Upsilon_k f_{E,k}^{\mathrm{o}-} \tag{94}$$

where

$$\Upsilon_k=\gamma_1(-1)^k+\gamma_2=-\frac{T_{L,0}^{i2w}[(t_0^-(-1)^k-r_0^+)R_{R,0}^{w2i}\mathrm{e}^{-k_0 l/2}+\mathrm{e}^{k_0 l/2}]}{(t_0^- t_0^+-r_0^- r_0^+)R_{L,0}^{w2i}R_{R,0}^{w2i}\mathrm{e}^{-k_0 l}-\mathrm{e}^{k_0 l}+r_0^- R_{L,0}^{w2i}+r_0^+ R_{R,0}^{w2i}} \tag{95}$$

Similar to Eq. (82), Υ_k can be approximated as

$$\Upsilon_k=\frac{T_{L,0}^{i2w}}{\mathrm{e}^{k_0 l/2}-rR\mathrm{e}^{-k_0 l/2}} \tag{96}$$

The peaks and troughs of $|\Upsilon_k|$ can be found through Eq. (83). Thus the oscillatory behaviour of the exciting force is the same as that of the hydrodynamic coefficient, as can be seen in Fig. 14 for the heave wave exciting force, together with Fig. 12 for the heave added mass and damping coefficient. Eq. (95) indicates that $f_{E,k}$ will oscillate against $|k_0 l|$ periodically at a given σ, as plotted in Fig. 15.

From Eqs. (81) and (95), it can be seen that the oscillatory behaviour for the hydrodynamic force will never diminish even when $l\to\infty$ at a given σ. This means that the motion of a body in an infinitely large polynya is not the same as that of a body on completely open free surface. This may seem to be a surprise. However, we may notice the radiation conditions in these two cases are given in Eqs. (9) and (10), (16) and (17) respectively, which are different. Different radiation conditions are expected to give different results. Physically, periodic motion state can be reached only after $t\to\infty$. Thus no matter how large l is, after sufficiently large time, the wave will arrive the ice edges which will give wave reflection. The reflected wave will eventually affect the body. We may also notice that if we increase σ at a fixed l while $\exp(k_0 l)$ is fixed, the result will be different. This is because A_j^-, $T_{L,0}^{i2w}$, R and r will vary as well now. In particular, as σ increases, for radiation problem A_j^- will tend to zero and the effect of ice sheet will disappear. For scattering problem $T_{L,0}^{i2w}$ will also tend to zero as σ increases, which means that no wave will transmit into the polynya, and the exciting force will become zero.

From Fig. 10 of Ren *et al.*[25], it was found that there was no standing wave in polynya due to the forced oscillation of body. This can be analyzed explicitly through Eq. (30). On the left hand side of the body, the complex wave amplitude of the wave along the x-axis is

$$C_k = \varepsilon_k^2 \tag{97}$$

and that opposite to the x-axis is

$$D_k = A_k^- + (-1)^i \varepsilon_k^2 t_0^+ + \varepsilon_k^2 r_0^- \tag{98}$$

Invoking Eq. (82), when σ increases, the above two equations can be further written as

$$C_k = \frac{A_k^- R}{\mathrm{e}^{k_0 l} - rR} \tag{99}$$

$$D_k = \frac{A_k^- \mathrm{e}^{k_0 l}}{\mathrm{e}^{k_0 l} - rR} \tag{100}$$

This indicates that we generally have $|C_k| < |D_k|$ unless when $|R| = 1$ at a total reflection which is most rare. Thus there is usually no standing wave in polynya due to the forced motion.

For the scattering problem, Eq. (46) shows that on the left hand side of body, the complex wave amplitude for the waves along and opposite to the x-axis are

$$C_0 = \gamma_2 \tag{101}$$

$$D_0 = \gamma_1 t_0^+ + \gamma_2 r_0^- \tag{102}$$

respectively. Then invoking Eq. (96), the above two equations can be written as

$$C_0 = \frac{T_{L,0}^{i2w}}{\mathrm{e}^{k_0 l/2} - rR\mathrm{e}^{-k_0 l/2}} \tag{103}$$

$$D_0 = \frac{T_{L,0}^{i2w} r_0^-}{\mathrm{e}^{k_0 l/2} - rR\mathrm{e}^{-k_0 l/2}} \tag{104}$$

At large σ we have $|r| = |r_0^+| = |r_0^-| \to 1$, which gives $|C_0| = |D_0|$. Thus there could be standing waves or at least approximately.

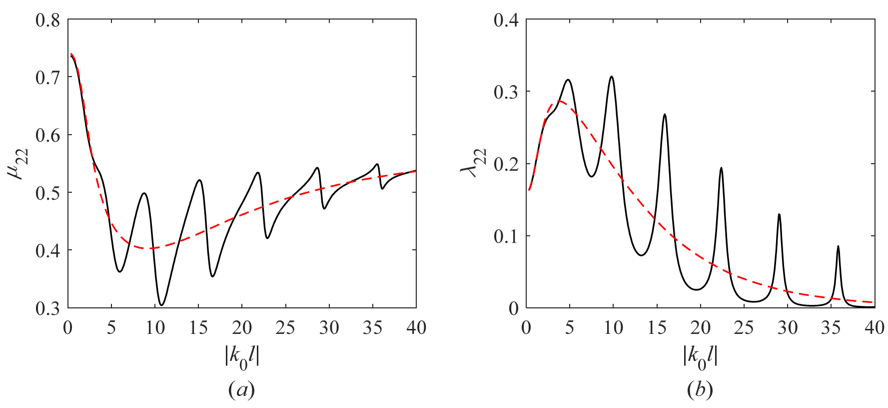

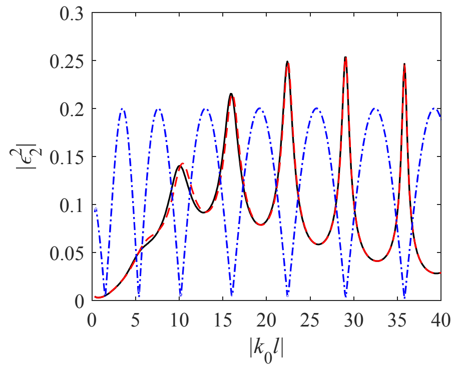

(*c*)

Fig. 12. Hydrodynamic coefficient in heave mode against $|k_0 l|$. (*a*) added mass; (*b*) damping coefficient; (*c*) $|\varepsilon_2^2|$. In (*a*) and (*b*), solid lines are for polynya while dashed lines are for open water. In (*c*), solid line is for Eq. (81), dashed line is for Eq. (82), and dash-dotted line represents $|S_\varepsilon(\omega)|/10$. ($a=1$, $b=0.5$, $H=10$, $x_1=-x_2=-5$, $h_1=h_2=0.1$, $d_1=d_2=0.09$, $m_1=m_2=0.09$, $L_1=L_2=4.5582$)

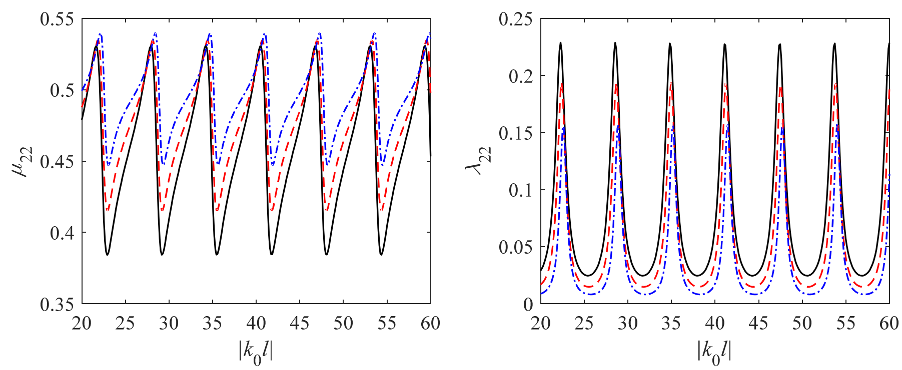

(*a*) (*b*)

Fig. 13. Hydrodynamic coefficient in heave mode with different σ against $|k_0 l|$. (*a*) added mass; (*b*) damping coefficient. Solid lines: $\sigma=1.94$; dashed lines: $\sigma=2.24$; dash-dotted lines: $\sigma=2.60$. ($a=1$, $b=0.5$, $H=10$, $x_1=-x_2=-5$, $h_1=h_2=0.1$, $d_1=d_2=0.09$, $m_1=m_2=0.09$, $L_1=L_2=4.5582$)

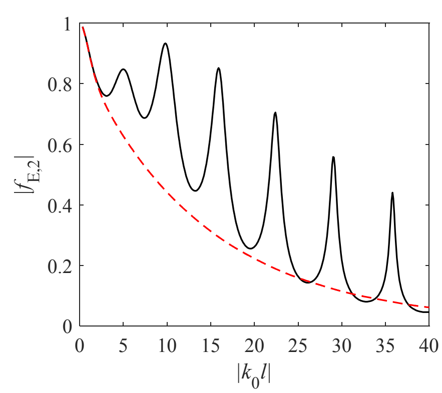

Fig. 14. Heave exciting force against $|k_0 l|$. Solid line is for polynya while dashed line is for open water. ($a=1$, $b=0.5$, $H=10$, $x_1=-x_2=-5$, $h_1=h_2=0.1$, $d_1=d_2=0.09$, $m_1=m_2=0.09$, $L_1=L_2=4.5582$)

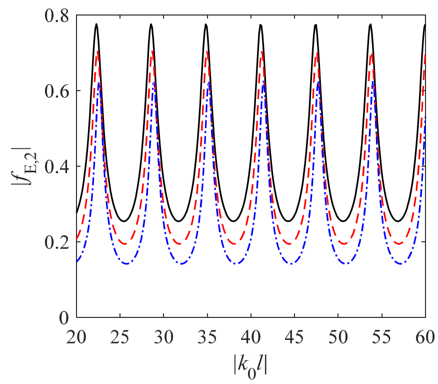

Fig. 15. Heave exciting force with different σ against $|k_0 l|$. Solid line: $\sigma=1.94$; dashed line: $\sigma=2.24$; dash-dotted line: $\sigma=2.60$. ($a=1$, $b=0.5$, $H=10$, $x_1=-x_2=-5$, $h_1=h_2=0.1$, $d_1=d_2=0.09$, $m_1=m_2=0.09$, $L_1=L_2=4.5582$)

D.2 Oscillation features of the body motion

Since the body is symmetric about $x=0$, the symmetric heave motion is fully decoupled from the anti-symmetric sway and roll motions. From Eq. (14) the complex heave motion amplitude can be obtained as

$$\frac{\alpha_2}{\alpha_0}=\frac{f_{E,2}}{-\sigma(m_{22}+\mu_{22})+\mathrm{i}\sqrt{\sigma}\lambda_{22}+C_{22}} \tag{105}$$

where the parameters are all nondimensional. Invoking Eqs. (40) and (54), this becomes

$$\frac{\alpha_2}{\alpha_0}=\frac{(\gamma_1+\gamma_2)f_{E,2}^{\mathrm{o}-}}{-\sigma(m_{22}+\mu_{22}^0)+\mathrm{i}\sqrt{\sigma}\lambda_{22}^0+2\sigma\varepsilon_2^2 f_{E,2}^{\mathrm{o}-}+C_{22}} \tag{106}$$

Resonance occurs when the exciting frequency coincides with one of the natural frequencies. For the undamped heave motion, we can find the natural frequencies when the inertial force is cancelled by the restoring force, or

$$-\sigma[m_{22}+\mu_{22}^0-2\,\mathrm{Re}(\varepsilon_2^2 f_{E,2}^{\mathrm{o}-})]+C_{22}=0 \tag{107}$$

This equation shows that the natural frequency for heave motion in polynya will be different from that for open water. Since both μ_{22}^0 and $\varepsilon_2^2 f_{E,2}^{\mathrm{o}-}$ are frequency dependent, Eq. (107) has to be solved numerically, for example done in Fig. 8 (*a*) of Ren *et al.*[25]. From the numerical solution it is found the natural frequency $\sigma\approx 1.19$ in the present case. A large peak can be found near this frequency (it should also be noticed that the damping will have some effect on this frequency), or resonance occurs. In addition to this peak, there are a series of local peaks in Fig. 16 (*a*), which are not commonly seen in the open water, as reflected by the dashed line in the figure. For large σ, we may use Eqs. (82) and (96) in (106). This gives

$$\frac{\alpha_2}{\alpha_0} = \frac{T_{L,0}^{i2w}\tilde{\alpha}_2 / \alpha_0}{\mathrm{e}^{k_0 l/2} - R(r - 2\sigma A_2^- \tilde{\alpha}_2 / \alpha_0)\mathrm{e}^{-k_0 l/2}} \tag{108}$$

where $\tilde{\alpha}_2$ is the complex heave motion for open water. Then the local extrema of $|\alpha_2|/\alpha_0$ can be found through the following equation

$$\begin{aligned} |U_2(\sigma)| &= |\mathrm{e}^{k_0 l/2} - R(r - 2\sigma A_2^- \tilde{\alpha}_2 / \alpha_0)\mathrm{e}^{-k_0 l/2}| \\ &= \sqrt{1 + |R(r - 2\sigma A_2^- \tilde{\alpha}_2 / \alpha_0)|^2 - 2\,\mathrm{Re}[R(r - 2\sigma A_2^- \tilde{\alpha}_2 / \alpha_0)\mathrm{e}^{-k_0 l}]} \end{aligned} \tag{109}$$

or more directly through

$$|S_2(\sigma)| = |1 + \mathrm{e}^{-k_0 l}\mathrm{e}^{\mathrm{i}\mathrm{Arg}[R(r - 2\sigma A_2^- \tilde{\alpha}_2/\alpha_0)]}| \tag{110}$$

Its peaks and troughs occur when δ equals

$$\delta_P^2 = 2n\pi - \beta - \mathrm{Arg}(r - 2\sigma A_2^- \tilde{\alpha}_2 / \alpha_0) \tag{111}$$

and

$$\delta_T^2 = 2n\pi + \pi - \beta - \mathrm{Arg}(r - 2\sigma A_2^- \tilde{\alpha}_2 / \alpha_0) \tag{112}$$

respectively. $|S_2(\sigma)|$ is plotted in Fig. 16 (*a*). It can been oscillations of $|\alpha_2|/\alpha_0$ and $|S_2(\sigma)|$ follow the same peaks and troughs, which explains its oscillatory behaviour. Eq. (108) also indicates that $|\alpha_2|/\alpha_0$ will oscillate with $|k_0 l|$ periodically at a given σ with the period of 2π, and the peaks and troughs occur when δ equals δ_P^2 and δ_T^2 respectively, as shown in Fig. 16 (*b*).

For the anti-symmetric coupled sway and roll motions, Eq. (14) provides

$$\frac{\alpha_1}{\alpha_0} = \frac{\vartheta_1}{\vartheta} \tag{113}$$

$$\frac{\alpha_3}{\alpha_0} = \frac{\vartheta_3}{\vartheta} \tag{114}$$

with

$$\vartheta_1 = [-\sigma m_{33} + (-\sigma\mu_{33} + \mathrm{i}\sqrt{\sigma}\lambda_{33}) + C_{33}]f_{E,1} - (-\sigma\mu_{13} + \mathrm{i}\sqrt{\sigma}\lambda_{13})f_{E,3} \tag{115}$$

$$\vartheta_3 = [-\sigma m_{11} + (-\sigma\mu_{11} + \mathrm{i}\sqrt{\sigma}\lambda_{11})]f_{E,3} - (-\sigma\mu_{31} + \mathrm{i}\sqrt{\sigma}\lambda_{31})f_{E,1} \tag{116}$$

$$\begin{aligned} \vartheta = {} & [-\sigma m_{11} + (-\sigma\mu_{11} + \mathrm{i}\sqrt{\sigma}\lambda_{11})][-\sigma m_{33} + (-\sigma\mu_{33} + \mathrm{i}\sqrt{\sigma}\lambda_{33}) + C_{33}] \\ & - (-\sigma\mu_{13} + \mathrm{i}\sqrt{\sigma}\lambda_{13})(-\sigma\mu_{31} + \mathrm{i}\sqrt{\sigma}\lambda_{31}) \end{aligned} \tag{117}$$

Then invoking Eq. (40) the undamped natural frequency can be found through

$$\begin{aligned} & \sigma\{[-(m_{11} + \mu_{11}^0) + 2\,\mathrm{Re}(\varepsilon_1^2 f_{E,1}^{\mathrm{o}-})][-(m_{33} + \mu_{33}^0) + 2\,\mathrm{Re}(\varepsilon_3^2 f_{E,3}^{\mathrm{o}-})] \\ & \quad - [-\mu_{13}^0 + 2\,\mathrm{Re}(\varepsilon_3^2 f_{E,1}^{\mathrm{o}-})][-\mu_{31}^0 + 2\,\mathrm{Re}(\varepsilon_1^2 f_{E,3}^{\mathrm{o}-})]\} + C_{33}[-(m_{11} + \mu_{11}^0) + 2\,\mathrm{Re}(\varepsilon_1^2 f_{E,1}^{\mathrm{o}-})] = 0 \end{aligned} \tag{118}$$

The numerical solution of this equation shows that there are multi natural frequencies for the coupled motions. Especially near $\sigma = 1.26$, the coupled motions are very large due to the equivalent damping level is very small at this frequency. Similar to the heave motion, there are also a series of local peaks and troughs in $|\alpha_1|/\alpha_0$ and $|\alpha_3|/\alpha_0$, which can be analyzed by substituting Eqs. (82) and (96) into Eqs. (113) and (114), or

$$\frac{\alpha_1}{\alpha_0} = \frac{T_{L,0}^{i2w}\tilde{\alpha}_1 / \alpha_0}{\mathrm{e}^{k_0 l/2} - [Rr - 2R\sigma(A_1^- \tilde{\alpha}_1 / \alpha_0 + A_3^- \tilde{\alpha}_3 / \alpha_0)]\mathrm{e}^{-k_0 l/2}} \tag{119}$$

$$\frac{\alpha_3}{\alpha_0} = \frac{T_{L,0}^{i2w}\tilde{\alpha}_3 / \alpha_0}{\mathrm{e}^{k_0 l/2} - [Rr - 2R\sigma(A_1^- \tilde{\alpha}_1 / \alpha_0 + A_3^- \tilde{\alpha}_3 / \alpha_0)]\mathrm{e}^{-k_0 l/2}} \tag{120}$$

Similar to Eq. (108), the local extrema for the coupled motions can be found through

$$|S_{13}(\sigma)| = |1 + \mathrm{e}^{-k_0 l}\mathrm{e}^{\mathrm{i}\mathrm{Arg}[Rr - 2R\sigma(A_1^- \tilde{\alpha}_1/\alpha_0 + A_3^- \tilde{\alpha}_3/\alpha_0)]}| \tag{121}$$

Its peaks and troughs occur when δ equals

$$\delta_P^{13} = 2n\pi - \beta - \mathrm{Arg}[r - 2\sigma(A_1^- \tilde{\alpha}_1 / \alpha_0 + A_3^- \tilde{\alpha}_3 / \alpha_0)] \tag{122}$$

and

$$\delta_T^{13} = 2n\pi + \pi - \beta - \mathrm{Arg}[r - 2\sigma(A_1^- \tilde{\alpha}_1 / \alpha_0 + A_3^- \tilde{\alpha}_3 / \alpha_0)] \tag{123}$$

respectively. It can be seen from Fig. 17 (*a*) and (*b*) that $|\alpha_1|/\alpha_0$ and $|\alpha_3|/\alpha_0$ follow the same peaks and troughs as $|S_{13}(\sigma)|$. Eqs. (119) and (120) indicate that $|\alpha_1|/\alpha_0$ and $|\alpha_3|/\alpha_0$ will also oscillate against $|k_0 l|$ for a given σ with period as 2π, and the peaks and troughs appear when δ equals δ_P^{13} and δ_T^{13} respectively, as reflected in Fig. 17 (*c*) and (*d*).

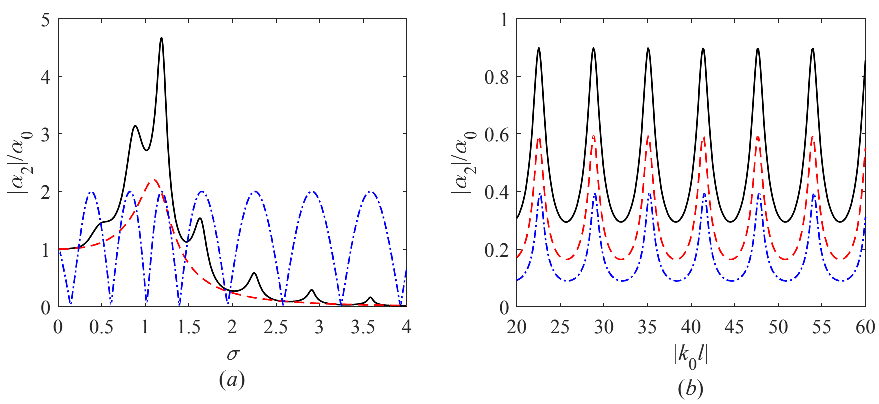

Fig. 16. Heave motion of a floating rectangle body. (*a*) $|\alpha_2|/\alpha_0$ against σ. (*b*) $|\alpha_2|/\alpha_0$ against $|k_0 l|$. In (*a*), solid line is for $x_1 = -x_2 = -5$ while dashed line is for open water, dash-dotted line represents $|S_2(\sigma)|$. In (*b*), solid line is for $\sigma = 1.94$, dashed line is for $\sigma = 2.24$, dash-dotted line is for $\sigma = 2.60$. ($a = 1$, $b = 0.5$, $m_{22} = 0.5$, $C_{22} = 1$, $H = 10$, $h_1 = h_2 = 0.1$, $d_1 = d_2 = 0.09$, $m_1 = m_2 = 0.09$, $L_1 = L_2 = 4.5582$)

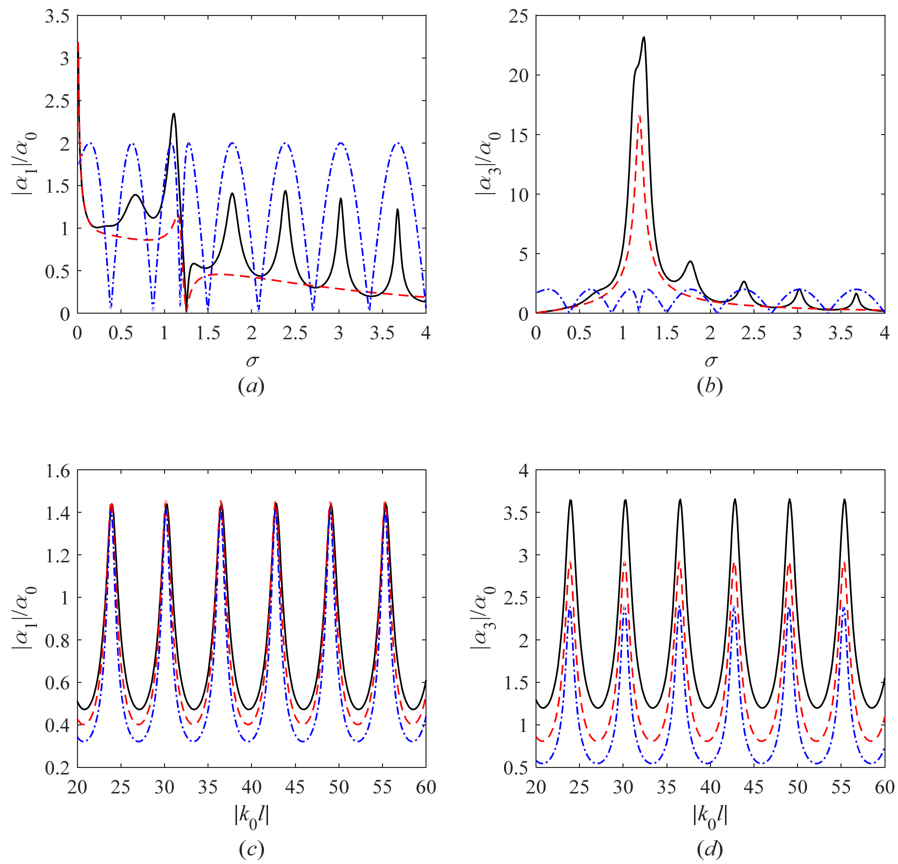

Fig. 17. Coupled sway and roll motions of a floating rectangle body. (*a*) $|\alpha_1|/\alpha_0$ against σ. (*b*) $|\alpha_3|/\alpha_0$ against σ. (*c*) $|\alpha_1|/\alpha_0$ against $|k_0 l|$. (*d*) $|\alpha_3|/\alpha_0$ against $|k_0 l|$. In (*a*) and (*b*), solid line is for $x_1 = -x_2 = -5$ while dashed line is for open water, dash-dotted line represents $|S_{13}(\sigma)|$. In (*c*) and (*d*), solid line is for $\sigma = 1.94$, dashed line is for $\sigma = 2.24$, dash-dotted line is for $\sigma = 2.60$. ($a = 1$, $b = 0.5$, $m_{11} = 0.5$, $m_{33} = 0.0521$, $C_{33} = 1/12$, $H = 10$, $h_1 = h_2 = 0.1$, $d_1 = d_2 = 0.09$, $m_1 = m_2 = 0.09$, $L_1 = L_2 = 4.5582$)

IV. CONCLUSIONS

A method based on wide spacing approximation has been proposed for the interaction of water wave with a body floating on a polynya. It has been found that this method based on the solutions for a floating body without ice sheet and for ice sheet/free surface without floating body can give accurate results for wave/body/ice sheet interaction problems. Extensive numerical results are provided, including the wave propagation across the polynya, and wave interaction with a submerged body and a floating body in polynya. The complex wave features, as well as hydrodynamic force and body response to the waves are analyzed. From these the following conclusions can be drawn:

(1) The method is accurate and efficient for the problems of wave propagation across a polynya,

and interaction with the submerged and floating bodies in polynya, including the long wave cases even though the method is based on the assumption of short waves.

(2) An explicit formula based on the present approximation has been found, which provides the discrete frequencies at which the wave reflection from a polynya confined between two semi-infinite ice sheets is zero. It occurs when the wavenumber K nondimensionalized by polynya width l is at $Kl = n\pi + \mathrm{Arg}(R)$ where n includes all integers which ensure $Kl > 0$ and R is the complex reflection coefficient of the free surface water wave by the semi-infinite ice sheet.

(3) The hydrodynamic force on a body in polynya has a highly oscillatory behaviour with the variation of the frequency. The mechanism for such oscillation has been investigated, which is found to be principally due to the waves being constantly reflected between the body and the ice sheet. It has been found when $Kl = 2n\pi + \mathrm{Arg}(Rr)$ or $Kl = 2n\pi + \pi + \mathrm{Arg}(Rr)$, where r is the reflection coefficient of the body in the open water without ice, the damping coefficient and wave exciting force tend to peak and trough values respectively, while the added mass tends to the value in the open water.

(4) The body motion in polynya, excited by an incoming wave, can experience resonance as in the open water, although the resonant frequency is different. In addition to the peak at the resonance, the motion amplitude also has many local peaks, or it also has oscillatory behaviour with respect to the frequency. These peaks are not necessarily due to the resonance at which the inertial force is cancelled by the restoring force. They are primarily linked to the oscillatory behaviours of the hydrodynamic coefficients and the excitation force, although their peaks and troughs may not be at the same frequency.

(5) At a given frequency, the hydrodynamic force and motion response of a body in polynya will vary with the polynya width periodically, and the period is $\Delta l = 2\pi / K$. This suggests that no matter how wide the polynya is, the effect of the ice sheet always exists. It means that when $l \to \infty$, the result does not tend to that in the open water without ice.

ACKNOWLEDGEMENT

This work is supported by Lloyd’s Register Foundation through the joint centre involving University College London, Shanghai Jiaotong University and Harbin Engineering University, to which the authors are most grateful. Lloyd’s Register Foundation helps to protect life and property by supporting engineering-related education, public engagement, and the application of research. This work is also supported by the National Natural Science Foundation of China (Grant No. 11472088)

REFERENCES

1. V. A. Squire, "Past, present and impendent hydroelastic challenges in the polar and subpolar seas," Philosophical Transactions 369, 2813 (2011).

2. E. M. Appolonov, K. E. Sazonov, A. A. Dobrodeev, N. Y. Klementieva, M. A. Kudrin, E. A. Maslich, V. O. Petinov and V. M. Shaposhnikov, "Studies for development of technologies to make a wide channel in ice," The 22nd International Conference on Port and Ocean Engineering under Arctic Conditions, Espoo, Finland, 9-13 June, (2013).

3. G. D. Q. Robin, "Wave Propagation through Fields of Pack Ice," Philosophical Transactions of the Royal Society B Biological Sciences 255, 313 (1963).

4. V. A. Squire, J. P. Dugan, P. Wadhams, P. J. Rottier and A. K. Liu, "Of ocean waves and sea ice," Annual Review of Fluid Mechanics 27, 115 (1995).

5. V. A. Squire, "Of ocean waves and sea-ice revisited," Cold Regions Science & Technology 49, 110 (2007).

6. C. Fox and V. A. Squire, "Reflection and transmission characteristics at the edge of shore fast sea ice," Journal of Geophysical Research Oceans 95, 11629 (1990).

7. C. Fox and V. A. Squire, "Coupling between the ocean and an ice shelf," Annals of Glaciology 15, 101 (1991).

8. C. Fox and V. A. Squire, "On the Oblique Reflexion and Transmission of Ocean Waves at Shore Fast Sea Ice," Philosophical Transactions of the Royal Society A Mathematical Physical & Engineering Sciences 347, 185 (1994).

9. T. Sahoo, T. L. Yip and A. T. Chwang, "Scattering of surface waves by a semi-infinite floating elastic plate," Physics of Fluids 13, 3215 (2001).

10. M. Meylan and V. A. Squire, "The response of ice floes to ocean waves," Journal of Geophysical Research Atmospheres 99, 891 (1994).

11. D. V. Evans and T. V. Davies, "Wave–ice interaction, Report 1313, Davidson Laboratory, Stevens Institute of Technology, New Jersey, ," (1968).

12. H. Chung and C. Fox, "Calculation of wave-ice interaction using the wiener-hopf technique," New Zealand J Math 31, 1 (2002).

13. N. J. Balmforth and R. V. Craster, "Ocean waves and ice sheets," Journal of Fluid Mechanics 395, 89 (1999).

14. L. A. Tkacheva, "Hydroelastic behavior of a floating plate in waves," Journal of Applied Mechanics & Technical Physics 42, 991 (2001).

15. L. A. Tkacheva, "The diffraction of surface waves by a floating elastic plate at oblique incidence," Journal of Applied Mathematics & Mechanics 68, 425 (2004).

16. H. Chung and C. M. Linton, "Reflection and transmission of waves across a gap between two semi-infinite elastic plates on water," The Quarterly Journal of Mechanics and Applied Mathematics 4, 305 (2005).

17. T. D. Williams and V. A. Squire, "Scattering of flexural–gravity waves at the boundaries between three floating sheets with applications," Journal of Fluid Mechanics 569, 113 (2006).

18. D. V. Evans and R. Porter, "Wave scattering by narrow cracks in ice sheets floating on water of finite depth," Journal of Fluid Mechanics 484, 143 (2003).

19. R. Porter and D. Evans, "Diffraction of flexural waves by finite straight cracks in an elastic sheet over water," Journal of fluids and structures 23, 309 (2007).

20. I. V. Sturova and L. A. Tkacheva, "Action of Periodic External Pressure on Inhomogeneous Ice Cover," The 32th International Workshop on Water Waves and Floating Bodies, Dalian, China, 23-26 April, (2017).

21. D. Das and B. N. Mandal, "Oblique wave scattering by a circular cylinder submerged beneath an ice-cover," International Journal of Engineering Science 44, 166 (2006).

22. I. V. Sturova, "Wave generation by an oscillating submerged cylinder in the presence of a floating semi-infinite elastic plate," Fluid Dynamics 49, 504 (2014).

23. I. V. Sturova, "The effect of a crack in an ice sheet on the hydrodynamic characteristics of a submerged oscillating cylinder," Journal of Applied Mathematics & Mechanics 79, 170 (2015).

24. I. V. Sturova, "Radiation of waves by a cylinder submerged in water with ice floe or polynya," Journal of Fluid Mechanics 784, 373 (2015).

25. K. Ren, G. X. Wu and G. A. Thomas, "Wave excited motion of a body floating on water confined between two semi-infinite ice sheets," Physics of Fluids 28, 20 (2016).

26. Z. F. Li, Y. Y. Shi and G. X. Wu, "Large amplitude motions of a submerged circular cylinder in water with an ice cover," European Journal of Mechanics-B/Fluids 65, 141 (2017).

27. Z. F. Li, Y. Y. Shi and G. X. Wu, "A hybrid method for wave interacting with a body floating on polynya confined between two semi-infinite ice sheets," The 32th International Workshop on Water Waves and Floating Bodies, Dalian, China, 23-26 April, (2017).

28. M. A. Srokosz and D. V. Evans, "A theory for wave-power absorption by two independently oscillating bodies," Journal of Fluid Mechanics 90, 337 (1979).

29. C. C. Mei, M. Stiassnie and K. P. Yue, "Theory and Applications of Ocean Surface Waves Part 1: Linear Aspects," World Scientific Publishing Co.pte.ltd.hackensack Nj (2005).

30. R. W. Yeung, "A Hybrid Integral-Equation Method for Time-Harmonic Free-Surface Flows," The 1st International Conference on Numerical Ship Hydrodynamics, Gaithersburg, Maryland, 20-22 October, (1975).

31. R. Eatock Taylor and J. Zietsman, "A comparison of localized finite element formulations for two-dimensional wave diffraction and radiation problems," International Journal for Numerical Methods in Engineering 17, 1355 (1981).
32. Z. F. Li, Y. Y. Shi and G. X. Wu, "Interaction of wave with a body floating on polynya between two semi-infinite ice sheets," Submitted for publication (2017).
33. M. Meylan and V. A. Squire, "Finite-floe wave reflection and transmission coefficients from a semi-infinite model," Journal of Geophysical Research Atmospheres 981, 12537 (1993).